Two-Photon and Fluorescence Spectroscopy and the Effect of Environment on the Photochemical Properties of Peridinin in Solution and in the Peridinin-Chlorophyll-Protein from *Amphidinium carterae*†

Sumie Shima,‡ Robielyn P. Ilagan,‡ Nathan Gillespie,‡ Brandi J. Sommer,‡ Roger G. Hiller,§ Frank P. Sharples,§ Harry A. Frank,*,‡ and Robert R. Birge*,‡

Department of Chemistry, University of Connecticut, 55 North Eagleville Road, Storrs, Connecticut 06269-3060, and School of Biological Sciences, Macquarie University, NSW 2109, Australia

Received: December 30, 2002; In Final Form: March 14, 2003

The ground and excited-state properties of peridinin in solution and in the peridinin-chlorophyll-protein (PCP) complex are studied by using one-photon and two-photon spectroscopy, solvent effects, and quantum theory. Two-photon excitation spectra, two-photon polarization data, and fluorescence spectra in CS_2 reveal three low-lying excited singlet states in peridinin: a lowest-excited $^1A_g{}^{*-}$-like state with a system origin at ∼16 200 cm^{-1}, a $^1B_u{}^{*+}$-like S_2 state with a system origin at ∼19 300 cm^{-1}, and a $^1B_u{}^{*-}$-like S_3 state with a system origin at ∼22 000 cm^{-1}. The $^1B_u{}^{*+}$-like S_2 state dominates the two-photon excitation spectrum of peridinin in solution and in PCP because of type II enhancement associated with a large oscillator strength ($f \approx 1.6$) coupled with a change in dipole moment upon excitation ($\Delta\mu \approx 3$ D). Thus, the two-photon spectrum looks very much like the one-photon spectrum although weak vibronic bands of the $^1A_g{}^{*-}$-like state are observed at ∼17, ∼18.1, and ∼19.2 kK in the two-photon spectrum of peridinin in CS_2. MNDO−PSDCI theory and solvent effect studies indicate that the S_1 ($^1A_g{}^{*-}$-like) state has a large dipole moment ($\mu_{aa} \approx 16$ D, $\Delta\mu \approx 8$ D) in both polar and nonpolar environments, much larger than the ground-state dipole moment [$\mu_{00} \approx 6$ (non polar media) − 8 (polar media) D]. Thus, the $^1A_g{}^{*-}$-like state is assigned as the charge-transfer state observed in previous studies. The suggestion that the charge-transfer character is induced in polar solvent is not supported by these studies. We conclude that some of the studies that have suggested an increase in the charge-transfer character of S_1 with solvent polarity are based on experiments that are more sensitive to $(\mu_{aa} - \mu_{00})\mu_{00}$ than $(\mu_{aa} - \mu_{00})$. Peridinin exists as a mixture of all-trans and 14-s-cis (single bond to allene moiety) conformers in ambient temperature hexane solution, with a predominance of the former. Polar solvents such as methanol and high-dielectric solvents such as CS_2 preferentially stabilize the all-trans conformer relative to the 14-s-cis. MNDO−PSDCI calculations on the minimized peridinin molecules within PCP indicate that most of the chromophores have excited state properties similar to those observed for the isolated all-trans chromophore. However, the chromophores occupying sites 612 and 622 are not only blue shifted but have inverted S_1 and S_2 singlet states. Our studies provide both support and additional perspective on the PCP energy transfer model proposed by Damjanovic et al. (*Biophys. J.* **2000**, *79*, 1695−1705) in which the peridinin molecules in these sites transfer energy to other peridinin chromophores rather than directly to chlorophyll. We conclude that the 612 and 622 sites optimize energy transfer by increasing the population of the lowest-excited $^1B_u{}^{*+}$-like state, which provides enhanced dipolar coupling to the remaining peridinin set. An analysis of the PCP complex spectrum in terms of component spectra of the pigments indicates that two peridinin molecules have unique, blue-shifted spectra.

Introduction

Photosynthetic organisms use antenna pigment−protein complexes for harvesting light energy and for transferring the excitation energy to the reaction center where it is converted into chemical potential.[1] Antenna pigment−protein complexes from dinoflagellates containing peridinin have been shown to exhibit exceptionally high (> 95%) energy transfer efficiencies between the carotenoid and chlorophyll (Chl).[2−6] Among the few antenna pigment−protein complexes that have been crystallized and solved to atomic resolution using X-ray or electron diffraction techniques[7−10] is the water-soluble peridinin-chlorophyll-protein (PCP) complex from the dinoflagellate, *Amphidinium carterae*.[11,12] The structure of this complex was solved to a resolution of 2.0 Å revealing a noncrystallographic trimer of polypeptides comprising the fundamental unit of the protein.[11,13] Each of the polypeptides has pseudo 2-fold symmetry and binds eight peridinin molecules and two Chl *a* molecules (Figure 1). van der Waals contact between the peridinins and Chl *a* molecules in the complex facilitates energy transfer between the pigments.[14] The elucidation of this structure has given rise to several investigations correlating the molecular

† Part of the special issue "A. C. Albrecht Memorial Issue".

* To whom correspondence should be addressed. Robert R. Birge or Harry A. Frank, Department of Chemistry, University of Connecticut, 55 North Eagleville Road, Storrs, CT 06269-3060. E-mail: rbirge@uconn.edu or harry.frank@uconn.edu.

‡ University of Connecticut.

§ Macquarie University.

10.1021/jp022648z CCC: $25.00
Published on Web 05/06/2003

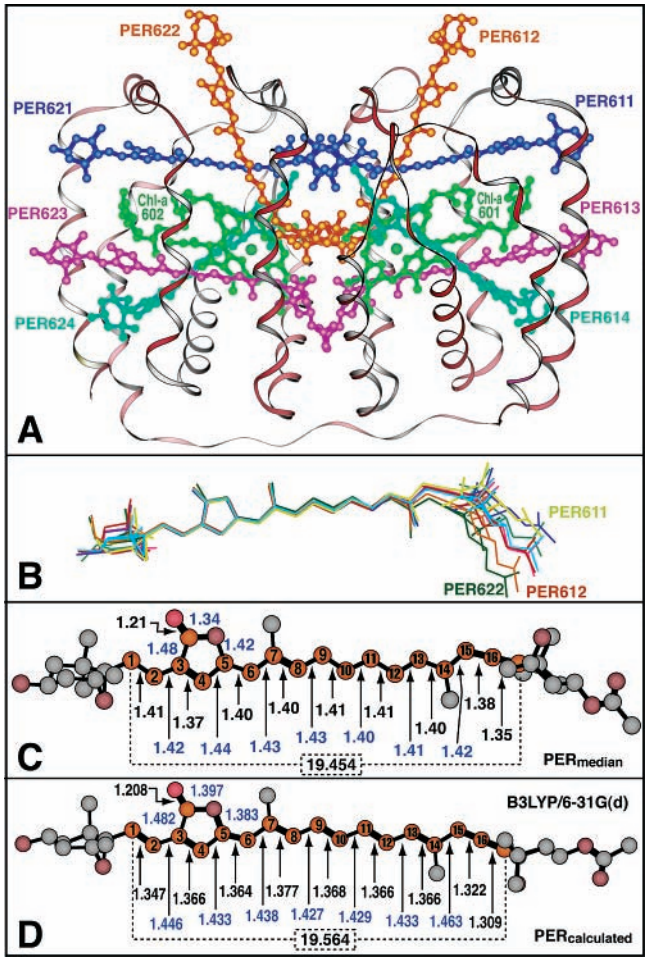

Figure 1. Structure of the pigments associated with one-third of the trimeric minimal unit comprising the PCP complex is shown in A based on PDB entry 1PPR (Hofmann, E.; Wrench, P. M.; Sharples, F. P.; Hiller, R. G.; Welte, W.; Diederichs, K. *Science* **1996**, *272*, 1788). The peridinin molecules are colored to reflect the pseudo 2-fold axis that runs vertically through the center of the protein. The peridinin molecules transfer energy to the Chl-*a* molecules shown in light green. Insert B shows the structures of all of the peridinin molecules oriented for maximal overlap in the polyene chain. A median structure of the peridinin molecules within the crystal is shown in C and compared to the lowest-energy vacuum structure based on density functional methods [B3LYP/6-31G(d)] in D.

features of the complex with its spectroscopic properties and attempting to rationalize its exceptionally high efficiency of energy transfer between peridinin and Chl *a*.[14−30]

The photochemical behavior of carotenoids and long-chain polyenes is dominated by the properties of the two lowest-lying excited singlet states. Because the properties of these states in low-symmetry, highly substituted polyenes can be understood by reference to the corresponding states observed under rigorous C_{2h} symmetry, it is common to use the C_{2h} symmetry labels for reference.[31−33] The lowest excited singlet state in long-chain linear polyenes, S_1, has $^1A_g{}^{*-}$-like symmetry and is optically forbidden under one-photon selection rules because the closed shell ground state has identical symmetry. The second excited singlet state in these polyenes, S_2, has $^1B_u{}^{*+}$-like symmetry and is strongly allowed under one-photon selection rules. This state is responsible for the strong λ_{max} absorption band observed in carotenoids. The superscript "+" and "-" labels refer to the configurational properties of the states with reference to the addition or subtraction of component excitations.[34] Minus states, such as the $^1A_g{}^{*-}$ state, are described to a first approximation in terms of the subtraction of two one-electron excitations. Minus states are "covalent" in character, a reference to a valence bond description involving a linear combination of bonding structures that have small amounts of charge separation. In contrast, "+" states are ionic in character and are described to a first approximation in terms of the addition of two one-electron excitations. Thus, "+" states are often intense because of the additive properties of the participating configurations. Ionic states are typically stabilized by a polar environment, whereas covalent states are relatively unaffected by the polarity of the polyene chain or environment.[35] In many respects, the properties of the excited states are determined more by the "ionic" (+) versus "covalent" (−) properties than the symmetric (g) versus unsymmetric (u) labels. The positions and dipolar properties of both the $^1A_g{}^{*-}$-like and $^1B_u{}^{*+}$-like states are important because the absorption properties are typically dominated by S_2, whereas the photochemical properties are dominated by S_1.[36] The challenge is to assign the energetic and dipolar properties of the S_1 state, because it is optically forbidden. Although this state can often be observed in fluorescence, and the properties deduced from an analysis of the fluorescence lifetime and emission profile, the emission takes place from a relaxed excited-state geometry. The Franck−Condon properties of the S_1 state are therefore not well-established, and it is often not possible to assign the location of the system origin. Finally, recent investigations have suggested that longer polyenes and carotenoids possess other electronic states, e.g., a $^1B_u{}^{*-}$-like state, between S_2 ($1^1B_u{}^{*+}$) and S_1 ($2^1A_g{}^{*-}$).[37−40] One-photon and two-photon absorption into $^1B_u{}^{*-}$ states is parity forbidden, and in linear polyenes, the $^1B_u{}^{*-}$ state is spectroscopically silent in both one and two photon spectroscopy. Birge and Pierce have shown, however, that this state becomes two-photon allowed when there are cis-linkages or polar groups in the polyene chain.[34]

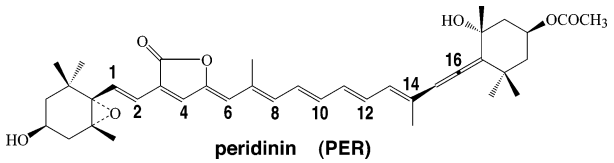

peridinin (PER)

Peridinin is a highly substituted carotenoid associated with the Peridiniales group of dinoflagellates.[41−43] As shown above, the molecule displays an atypical C_{37} carbon skeleton for carotenoids and possesses an allene group and a lactone ring in conjugation with the π-electron conjugated system.[44] We have labeled the carbon atoms along the polyene chain using a simplified numbering scheme to facilitate discussion of the conformers. Note that the carbonyl group of the lactone ring is also part of the polyene conjugated network. These features, in addition to epoxy and acetate functional group substitutions, suggest no symmetry at all. Yet, the steady-state absorption and fluorescence spectra of peridinin in nonpolar solvents are very similar to those usually observed in carotenoids. Peridinin has a strong absorption band in the visible region that shifts to lower energy with increasing solvent polarizability.[29] This behavior identifies this band with the strong dipole-allowed $^1A_g{}^{*-} \rightarrow {}^1B_u{}^{*+}$-like transition. The fluorescence spectrum of peridinin is significantly red-shifted from its absorption spectrum indicating that the emission originates from a lower-lying singlet state, which is consistent with a $^1A_g{}^{*-}$-like state.[29,45] This observation is typical of carotenoids and polyenes having more than three but less than nine carbon−carbon double bonds.[46] The dynamics of the S_1 state and the $S_1 \rightarrow S_n$ transient absorption spectrum of peridinin are not typical of carotenoids, however. Peridinin exhibits a pronounced solvent dependence of its $S_1 \rightarrow S_n$

transient absorption spectrum and its lowest excited singlet state lifetime with values ranging from ~160 ps in nonpolar solvents to ~10 ps in polar solvents.[29] It was hypothesized that this unorthodox behavior of peridinin could be explained by the presence of an intramolecular charge transfer state in its excited-state manifold.[29] It was suggested that the charge transfer state is derived from the presence of the lactone ring in the π-electron conjugation of peridinin. This idea was supported by both steady-state and transient spectroscopic studies on peridinin and other carotenoids containing either lactone rings or carbonyl substituents as part of the conjugated chain.[20,30,47,48] Yet, questions still remain regarding the function of this putative charge transfer state and how it should be viewed. Is it a discrete state populated via nonradiative deactivation from either S_2 or S_1, or is it so strongly coupled to S_2 or S_1, or both, that it cannot be distinguished? What is its precise role in determining the spectral properties and dynamics of peridinin and related molecules and in controlling energy transfer to chlorophyll in the PCP complex?

Data from recent studies by Zingmantas et al.[47,48] of the dependence of the dynamics of the excited states of peridinin on excitation wavelength, temperature, and solvent viscosity are interpreted in terms of mixing between the charge transfer state and S_1 that becomes stronger with increasing solvent polarity. The model proposed by these authors is consistent with that of Frank et al. [30] which invokes a CT state-induced perturbation of the potential energy surface of the S_1 state that leads to alterations in spectral line positions, band intensities, quantum yields of emission, and dynamics of the excited state depending on the solvent. The authors suggest that coupling between the S_1 and charge transfer states should be considered so strong that the states cannot be distinguished and that only a single S_1/CT electronic state exists whose dipole moment, or charge-transfer character, increases with solvent polarity. Spectroscopic signals associated with an unperturbed S_1 state are observed when peridinin is dissolved in nonpolar solvents, and signals associated with a strongly perturbed S_1 state are observed when polar solvents are used. These investigators have also proposed that peridinin adopts different spectral forms when hydrogen bonding solvents are used. The basis for this conclusion derives from the observation that when methanol or ethylene glycol is used as a solvent the singlet state lifetime of peridinin exhibits a dependence on excitation wavelength. The lifetime of the lowest-lying singlet state of peridinin, which is on the order of 5−10 ps in highly polar solvents, is found in methanol or ethylene glycol to be approximately a factor of 2 longer when it is excited below 525 nm than when it is excited above 530 nm. This effect is not observed when *n*-hexane or acetonitrile, solvents incapable of hydrogen bonding, are used. Zigmantas et al.[48] suggest that the broad absorption spectra of peridinin seen in polar solvents are due to interactions between the molecule and the electric field of the solvent, with an additional effect from hydrogen bonding, when such is present. These authors also believe that the presence of the CT state in the excited-state manifold of peridinin promotes dipolar interactions with Chl in the PCP complex and facilitates energy transfer via a dipole mechanism.[47]

In this paper, we examine the properties of peridinin in solution and in the PCP complex, by using linear and nonlinear laser spectroscopy, solvent effect studies and quantum theory. We compare and contrast our results with those from recent one-photon[47,48] and two-photon[49] studies. By collecting two-photon polarization data and comparing the results with predictions from MNDO−PSDCI molecular orbital theory, we are able to assign the location and approximate symmetries of the three lowest-lying excited singlet states. We examine our theoretical prediction that there are two peridinin molecules within PCP that occupy unique sites that shift their absorption spectra to the blue and invert the $^1B_u{}^{*+}$-like and $^1A_g{}^{*-}$-like excited singlet states. Finally, we examine the current models that propose that the lowest-lying $^1A_g{}^{*-}$-like excited singlet state has charge-transfer character.[29,30,48]

Materials and Methods

Sample Preparation. The PCP complex was prepared as in Sharples et al.[50] Pigments were extracted from PCP by the procedure of Martinson and Plumley[51] except that *n*-butanol was used in place of *sec*-butanol. Peridinin was initially separated from Chl *a* using an alumina column equilibrated with *n*-hexane containing increasing percentages from 0.0% to 35.0% acetone as an eluant. The absorption spectra of the fractions were obtained using a Cary 50 UV/vis spectrometer. The fraction containing peridinin had a λ_{max} of 475 nm and was obtained from the alumina column after elution with approximately 30.0% acetone in *n*-hexane. The peridinin was dried completely with a gentle stream of nitrogen prior to further purification using high performance liquid chromatography (HPLC).

Peridinin was further purified by HPLC carried out using a 4.6 × 250 mm (C30) YMC carotenoid column (5 μm) on a Millipore Waters 600E instrument equipped with a photodiode array detector. The HPLC instrument was operated using Waters Millenium software version 3.20. The peridinin was chromatographed using an isocratic mixture of 11:89 v/v methyl-tert-buthyl ether (MTBE):methanol with the flow rate of 1.0 mL/min. The chromatographic separation was monitored at 475 nm. The fraction containing peridinin appeared at a retention time of approximately 5 min and was collected and dried using a gentle stream of nitrogen.

Spectroscopic Methods. *Linear Spectroscopy.* Absorption spectra of peridinin were recorded on a Cary 50 UV/Vis spectrometer at either room temperature or 10 K. The steady-state fluorescence experiments were carried out at room temperature using an SLM Instruments, Inc. model 8000C spectrofluorimeter equipped with a grating having 1500 grooves per mm and a Hamamatsu R636 photomultiplier (PMT) tube. A 450 W ozone free OSRAM XBO Xenon arc lamp was used for excitation. An SLM Instrument model WCTS-1 thermostatically cooled housing was used to reduce the PMT dark current. The sample was excited at 486 nm and the emission passed through a 495 nm high-pass cutoff filter into a detection monochromator positioned 90° to the excitation beam. The band-pass setting for the excitation monochromator was 16 nm and for the detection monochromator was 4 nm. The emission spectrum was scanned at a relatively low amplifier gain and PMT voltage to obtain the maximum signal intensity that would occur in that spectral range. The wavelength at which the maximum signal was observed was used by the software to set the PMT voltage and amplifier gain to achieve a signal that registered 80% of the saturation maximum of the PMT. The spectrum was then scanned using these instrumental parameters. A spectral scan of a solvent blank was also taken under the same experimental conditions and was subtracted from the spectral trace of the sample. A correction curve generated by a spectral Irradiance 45 W quartz-halogen tungsten coiled filament lamp standard was used to correct the fluorescence spectra for the instrument response.

The absorption spectra of Chl *a*, peridinin, and the PCP complex presented in Figure 9 were recorded at 10 K. The PCP

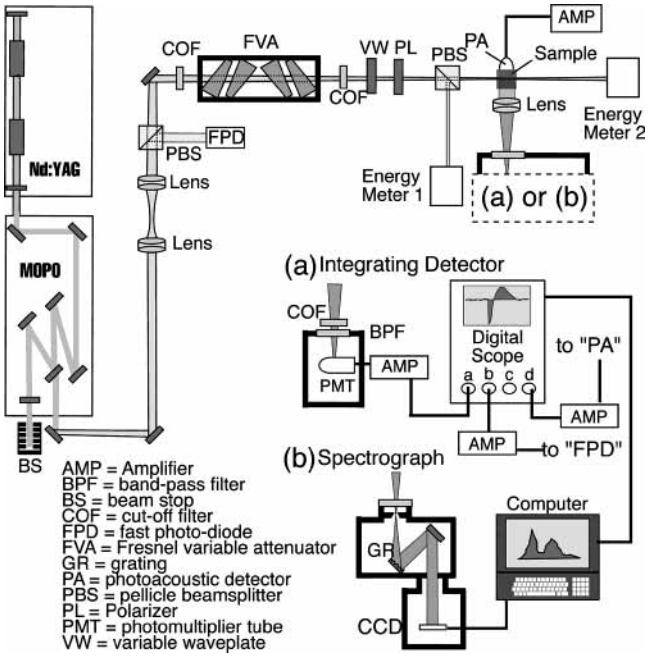

Figure 2. Schematic of the two-photon spectroscopy apparatus used to obtain the nonlinear optical spectra and polarization data reported here. The system can simultaneously observe two-photon induced fluorescence and photoacoustic signals, but all of the data reported here are based on the fluorescence, which provided a better signal-to-noise ratio. Polarization ratios are obtained by using the variable waveplate to convert the linearly polarized into circularly polarized light.

complex was suspended in 50 mM tricine, 20 mM KCl buffer, at pH 7.5 and was mixed with an equal volume of glycerol prior to freezing in a 1 cm × 1 cm polymethacrylate plastic cuvette in a Janis helium vapor flow model STVP100 cryostat. The Chl *a* and peridinin were both dissolved in 2-MTHF which formed a clear glass at 10 K. The summation of the absorption spectra of the pigments was carried out using Origin version 7.0 software.

Nonlinear Spectroscopy. Two-photon excitation (TPE) spectra were acquired at room temperature using the two-photon spectrophotometer shown in Figure 2. The sample volume was ~1 mL, and the concentration of the solute was adjusted to provide approximately 6 OD at λ_{max} for a 1 cm path length. The excitation source was a narrow-line-width (<2 cm^{-1}) optical parametric oscillator (Spectra Physics MOPO−SL) pumped by the third harmonic of a Nd:YAG pulsed laser system (Spectra Physics Quanta-Ray PRO 250−10). The source beam, tunable from 750 to 1800 nm, was led into a variable high energy attenuator (935−10) via high energy broadband mirrors (10D20-ER-2-PF, Newport Corp.). A small fraction (2−10%) of the attenuated beam was sampled by a high sensitivity pyroelectric energy meter (Coherent LM-P209, Labmaster Ultima data acquisition unit (DAQ)) via either a pellicle beam splitter (PBS-2, Newport) or an optical quality glass window (BK7 glass, Escoproducts). A second energy meter (Ophir Optronics BB-50, Laserstar DAQ) monitored the excitation energy transmitted through the sample. A calibration curve was collected with nothing in the sample holder to correlate the readings from the two meters, under the assumption that they were directly proportional at each wavelength. A lens focused the emission from each sample through an interference filter (centered at 705 nm (72 nm fwhm, Melles-Griot #03FIB016) for peridinin and 645 nm (75 nm fwhm, Melles-Griot #03FIB014) for the PCP complex) onto a red-enhanced photomultiplier tube (PMT; Hamamatsu Corp. R928). A fast photodiode assembly (Thor Labs D400FC) measured the temporal intensity profile of the beam. The signals from the PMT and the photodiode were processed with a digitizing oscilloscope (HP Infinium), and the average of 100 such signals was recorded for each data point, along with the average energy of 100 pulses from each of the meters. The background (solvent) and sample data were collected in pairs at each wavelength to minimize possible error from minor variations in laser performance. The two-photon polarization data were collected by dividing the two-photon signal for circularly polarized light by the two-photon signal for parallel polarized light. The latter polarization is the intrinsic output of the optical parametric oscillator (Spectra Physics MOPO−SL). Two identical variable waveplates (New Focus # 5540) were used on a track mount (Newport # PRL-24, PRC-1, and PRC-3) to create circularly polarized light. The signal for circularly polarized light and for linearly polarized light were collected in pairs at each wavelength to minimize experimental variation. At each new wavelength, the sample was removed, and one of the variable waveplates was set to produce circular light. To remove any remaining linear component in the beam exiting the waveplate, the polarizer immediately following it was adjusted until the power meter displayed the minimum incident energy. The sample was then removed again, and the track mount was moved to introduce the same waveplate with no retardance. In this case, the polarizer and attenuator were adjusted to produce a linear beam of approximately the same energy as the circular one. All two-photon data are plotted as a function of laser wavelength divided by two and corrected for laser intensity by dividing by the square of the laser intensity.

Theoretical Methods. Ground-state equilibrium geometries and properties were calculated using Gaussian 98, B3LYP density functional methods, and a 6-31G(d) basis set.[52] Excited-state properties were calculated by using MNDO−PSDCI molecular orbital theory with full single and partial double configuration interaction over the π system of the polyene chromophore.[53] These semiempirical molecular orbital procedures have been shown to provide accurate transition moments of long-chain linear, substituted polyenes and carotenoids.[54−56] We have developed spectroscopic parametrizations that work with the MNDO, AM1, or PM3 Hamiltonians.[53−55,57−61] In most cases, the MNDO−PSDCI method is most accurate when the PM3 Hamiltonian is selected, because this parametrization generates a more correlated excited state description. However, we have found that the use of density functional methods tends to slightly overcorrelate the ground state, and that this problem can be partially offset by using the AM1 Hamiltonian. Thus, the present calculations use the AM1 Hamiltonian when the ground-state geometry is generated via density functional methods. Otherwise, we use the PM3 Hamiltonian for the MNDO−PSDCI calculations.

Two-photon absorptivities were calculated by using the perturbation methods of Masthay et al.[62] The summation was over the 60 lowest energy excited singlet states from the MNDO−PSDCI configuration interaction analysis including the initial (ground) and final states.[63] The two-photon absorptivities were calculated assuming an identical normalized line-shape function for all transitions of $g_{max} = 10^{-14}$ s, which corresponds to a Gaussian absorptivity profile with a full-width at half-maximum of about 3000 cm^{-1}. False resonances or failed convergence were monitored and are noted where applicable. Perturbation methods and fixed line-shape functions can provide only approximate values for the two-photon absorptivities, but we anticipate that the relative values and the polarization ratios are more reliable.

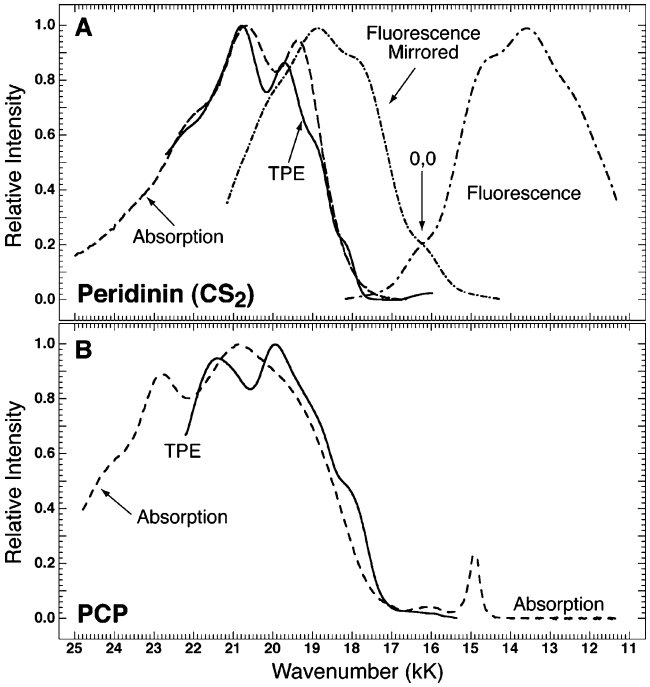

Figure 3. Two-photon spectra of peridinin (CS_2) and PCP (50 mM Tricine/20 mM KCl aqueous buffer) compared to the one-photon absorption spectra. The two-photon excitation (TPE) signal is an average of four scans using linearly polarized excitation, is corrected for laser pulse energy fluctuations by dividing by laser intensity squared, and is plotted as a function of excitation wavelength divided by two. The fluorescence spectrum of peridinin, which is associated with the lowest-lying $^1A_g{}^{*-}$-like state, is also shown along with its mirror image for reference. The mirror image provides a rough estimate of the Franck−Condon profile of the $^1A_g{}^{*-}$-like absorption spectrum.

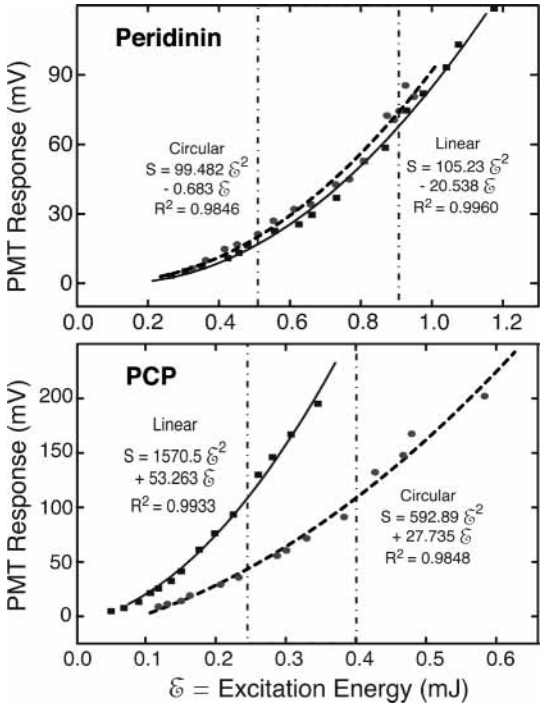

Figure 4. Regression analysis of the two-photon character of the fluorescence excitation signals (PMT = Photomultiplier; Figure 2a) for peridinin and PCP using both linear and circularly polarized laser excitation. Although the least-squares fits are dominated by the energy squared term, some linear (one-photon) character is present due to contributions from random noise and scattered laser light. The excitation energy dependence of peridinin (top) was measured at 1100 nm and monitored at 645 nm and of PCP (bottom) at 1020 nm and monitored at 705 nm. Plots of intensity vs excitation energy squared showed linear relationships with $R^2 > 0.99$ for all cases (data not shown). The vertical dashed lines delineate the pulse energy regions used for collecting the excitation and polarization spectra shown in Figures 3 and 5.

Solvent effects were studied theoretically by using Mopac2000 and both conductor-screening methods (COSMO)[64] and the more rigorous, but less flexible, methods proposed by Miertus, Scrocco, and Tomasi (MST).[65,66] The COSMO method allows geometry optimization in the continuum field introduced by the solvent reaction field, and the AM1 parametrization was used. The MST method was used to calculate the solvent shift associated with fixed geometries generated via COSMO minimizations in the same solvent.

Results and Discussion

We divide our discussion into four sections for convenience. First, we present the two-photon excitation and polarization spectra of peridinin in solution and in PCP. Second, we use MNDO−PSDCI molecular orbital theory to analyze the two-photon results and help assign the level ordering and photophysical properties of the low-lying excited singlet state manifold. Third, we investigate the impact of the protein environment on the excited state properties of peridinin and evaluate the possibility that two of these chromophores occupy photophysically unique sites. We conclude with an examination of solvent effects on peridinin and discuss the characteristics of the charge-transfer state that is observed in polar solvents.

Two-Photon Excitation and Polarization Spectra. The two-photon excitation spectra of peridinin in CS_2 and PCP in aqueous buffer are shown in Figure 3. The spectra are averages of four scans and were smoothed using a 4 nm slit function. We verified the two-photon character of the spectra and verified the lack of in situ second harmonic generation by using the methods and procedures discussed previously.[67,68] Examples of the quadratic dependence of the signals for both solutes are shown in Figure 4. We selected CS_2 as the solvent for peridinin because it is nonpolar and has a high refractive index. As discussed below, this solvent preferentially stabilizes the all-trans conformer and maintains the vibronic structure in the absorption and emission bands. This solvent is useful for two-photon spectroscopy because it does not have strong vibrational overtones in the region from 800 to 1300 nm.

The response of the two-photon signal to polarized light not only provides an additional test of the origin of the two-photon signal but also provides insight into the symmetry of the electronic state accessed via the two-photon process. The two-photon polarization ratio is defined as the two-photon signal for circularly polarized light divided by that observed for linearly polarized light, assuming that the two photons are traveling in the same direction along the same axis.[34,62,69] The two-photon polarization ratio was collected for both peridinin and PCP, and the results are shown in Figure 5.

Two-photon spectroscopy is normally viewed as a method of inverting the one-photon selection rules and allowing the direct spectroscopic study of forbidden states. Thus, one-photon forbidden states, such as the low-lying $^1A_g{}^{*-}$-like state, are now two-photon allowed via a type I process (Figure 6). The two-photon spectroscopy of nonpolar molecules such as benzene[69] and diphenyl butadiene,[70] and many slightly polar molecules such as vitamin A (all-trans retinol)[71] and substituted hexatrienes (isotachysterol),[72] can be analyzed in terms of type I behavior. However, if a one-photon allowed state undergoes a large change in dipole moment, this state can also be two-photon allowed via a type II process (Figure 6).[63,73] The importance of

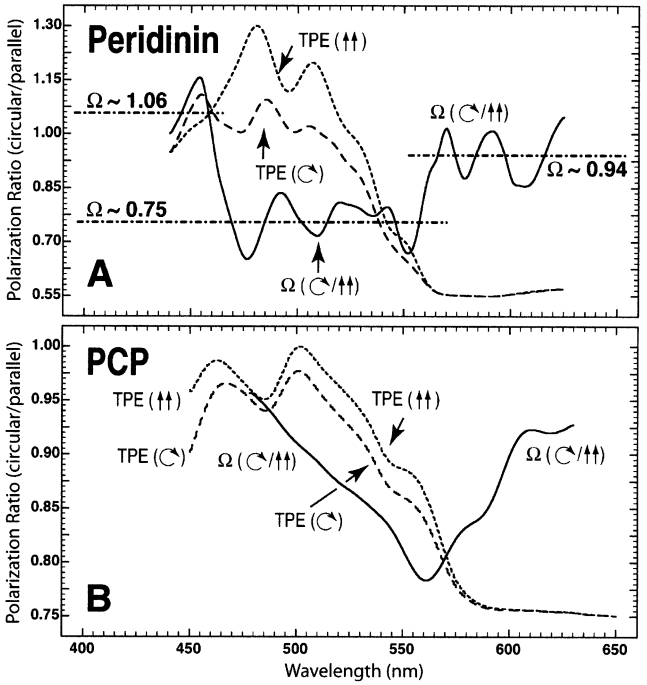

Figure 5. Polarization ratio, defined as the two-photon signal for circularly polarized light divided by the signal for linearly polarized light, plotted for peridinin in CS_2 (A) and PCP in buffer (B). The two-photon excitation spectra are shown using dashed lines for comparison. Three distinct polarization regions are delineated for peridinin.

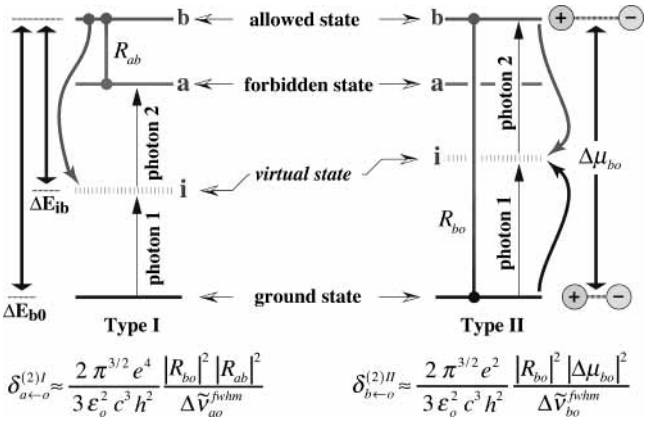

Figure 6. Two-photon absorption process which can take place via one of two mechanisms. The type I process (left) is important for excited states which are one-photon forbidden, labeled "a" in the diagram. The properties of the intermediate state are mediated by a nearby strongly one-photon allowed state, b, which exhibits large transition lengths between the final state (R_{ab}) and the ground state (R_{b0}). A strongly allowed one-photon state can also be a two-photon allowed state via a type II process (right) if it undergoes a change in dipole moment upon excitation ($\Delta\mu_{b0}$). The equations shown are based on the single intermediate state approximation and predict the maximum two-photon absorptivities for excited states with full-widths at half-maxima of $\Delta\tilde{\nu}^{fwhm}$. The above equations assume further that both photons have parallel polarization, parallel propagation and equal energy.

type II processes in proteins was first shown experimentally in a two-photon double-resonance study of the $^1B_u{}^{*+}$-like state in bacteriorhodopsin.[74] More recently type II processes have been shown to be important in studies of PCP and the carotenoid, peridinin.[49] Peridinin is a particularly interesting chromophore for two-photon studies because it has a lowest-lying $^1A_g{}^{*-}$-like state that shows evidence of charge-transfer character.[29,47,48] This behavior is contrary to the normal notion of $^1A_g{}^{*-}$-like states as being covalent states with dipole moments similar to the ground state.

The first observation that can be made regarding the two-photon spectra of both peridinin and PCP is that there is considerable coincidence between the one-photon absorption and two-photon excitation spectra. This observation has been made before[49] and is evidence of significant type II enhancement of the two-photon absorption process. This observation suggests that the strongly allowed $^1B_u{}^{*+}$-like state exhibits a dipole moment change upon excitation of greater than 2D. We will be able to more accurately quantify this with reference to the theoretical simulations outlined in the next section. However, there are vibronic features observed in the two-photon spectra of both systems that do not have a corresponding feature in the one-photon absorption spectra. These are most apparent on the red edges of the peridinin and PCP spectra (Figure 3). Previous studies have provided strong evidence for a lowest-lying $^1A_g{}^{*-}$-like state below the $^1B_u{}^{*+}$-like state responsible for the strong λ_{max} absorption band.[20,21,29,30,49] We suggest that the vibronic bands on the red edge are associated with a $^1A_g{}^{*-}$-like state. Further support for this hypothesis is provided by an analysis of the response of the two-photon spectrum to the polarization of the excitation beam (see below).

The ratio of the two-photon excitation signal for circularly polarized light divided by that for linearly polarized light is plotted in Figure 5. Although the polarization ratio for peridinin displays a reproducible vibronic structure, the ratio for PCP is broad and shows minimal vibronic development. Three distinct regions can be observed for peridinin and are delineated by using horizontal dashed lines in Figure 5A.

To understand the origin of the polarization response, we examine the simplified models for the two-photon absorptivity introduced in Figure 6. The single intermediate state approximation for the two-photon absorptivity can be written to explicitly include the influence of light polarization. The maximum absorptivity of a final state, *f*, via excitation of two photons of energy ΔE_λ via a type I two-photon excitation is[68]

$$\delta^{(2)I}_{f\leftarrow 0} = \frac{\pi^2 e^4 g_{max}}{60\,\epsilon_0^2 c^2 h^2}\frac{\Delta E_\lambda^2}{(\Delta E_{i0} - \Delta E_\lambda)^2}|R_{i0}|^2|R_{fi}|^2 \times \{(a+b)\cos^2\theta_{RR} + b\} \quad (1)$$

where g_{max} is the maximum value of the line-shape function (see below), ΔE_{i0} is the transition energy of the intermediate state, R_{i0} is the transition length from the ground state to the intermediate state, R_{fi} is the transition length from the intermediate state and the final state, θ_{RR} is the angle between the two transition lengths, and *a* and *b* are integers that define the polarization and propagation characteristics of the excitation beam. Parallel light with parallel propagation is represented using $a = 8$ and $b = 8$, whereas light of circular polarization in the same sense with parallel propagation is represented using $a = -8$ and $b = 12$. Values for other cases can be found in Table 1 of ref 62. The maximum absorptivity of a final state, *f*, via excitation of two photons of energy ΔE_λ via a type II two-photon excitation is[68]

$$\delta^{(2)II}_{f\leftarrow 0} = \frac{4\pi^4 e^2 g_{max}}{15c^2h^2}|R_{f0}|^2(\Delta\mu_{f0})^2\{(a+b)\cos^2\varphi_{R\Delta\mu} + b\} \quad (2)$$

where R_{f0} is the transition length from the ground state to the final state, $\Delta\mu_{f0}$ is the change in dipole moment between the ground and the final state, and $\varphi_{R\Delta\mu}$ is the angle between the

TABLE 1: Analysis of the Lowest Three Excited States of Peridinin Based on MNDO-PSDCI Calculations[a]

			ΔE		$\langle A \rangle$	$\langle B \rangle$	$\langle C \rangle$	$\langle D \rangle$		$\Delta\mu$	$\Delta\alpha$	DCI
conform	S_n	sym	eV	f	GM	GM	GM	GM	Ω	D	Å^3	%
all-trans	S_1	A_g^-	1.96	0.23	20.79	11.62	23.24	9.17	1.12	7.49	51.60	48
all-trans	S_2	B_u^+	2.39	1.68	489.97	219.46	438.92	270.51	0.90	2.16	179.10	21
all-trans	S_3	B_u^-	2.80	0.23	23.57	11.82	23.63	11.75	1.00	3.69	27.00	53
6-s-cis	S_1	A_g^-	1.86	0.15	53.66	31.28	62.55	22.39	1.17	5.79	42.90	47
6-s-cis	S_2	B_u^+	2.25	0.96	23.51	5.55	11.10	17.96	0.47	1.55	132.70	22
6-s-cis	S_3	B_u^-	2.68	0.11	46.53	29.77	59.54	16.76	1.28	1.81	16.60	56
multicis[b]	S_1	A_g^-	1.86	0.17	63.14	37.09	74.18	26.05	1.17	5.14	44.40	48
multicis	S_2	B_u^+	2.25	1.03	105.45	53.56	107.12	51.89	1.02	2.21	131.90	22
multicis	S_3	B_u^-	2.66	0.11	6.33	1.24	2.49	5.09	0.39	1.26	20.00	56

[a] The ground-state geometry was calculated for vacuum using Gaussian 98 and density functional methods [B3LYP/6-31G(d)]. The first column gives the conformation, where *multicis* indicates the 2,6,10,14-s-cis conformer, and the remaining columns are defined as follows: S_n (singlet manifold number), sym (approximate symmetry based on C_{2h}), ΔE (transition energy), f (oscillator strength), $\langle A \rangle$ (two-photon absorptivity for two photons linearly polarized with parallel propagation), $\langle B \rangle$ (two-photon absorptivity for two photons linearly polarized with perpendicular polarization), $\langle C \rangle$ (two-photon absorptivity for two photons circularly polarized in the same sense with parallel propagation), $\langle D \rangle$ (two-photon absorptivity for two photons circularly polarized in the opposite sense with parallel propagation), Ω ($\langle C \rangle / \langle A \rangle$, the polarization ratio), $\Delta\mu$ (excited-state dipole moment minus ground-state dipole moment), $\Delta\alpha$ (excited state polarizability minus ground state polarizability), DCI (percentage of doubly excited character in the excited singlet state CISD wave function). [b] multicis indicates the 2,6,10,14-s-cis conformer as shown in Figure 10B.

vectors R_{f0} and $\Delta\mu_{f0}$. The maximum line shape function, g_{max}, is defined by the shape of the two-photon absorption band profile and can be estimated by using[62]

$$g_{max} = \left[\frac{4 \ln 2}{\pi (c \Delta \tilde{\nu}_{f0}^{fwhm})^2}\right]^{1/2} \quad (3)$$

where $\Delta\tilde{\nu}_{f0}^{fwhm}$ is the full-width at half-maximum of the final state in wavenumbers (g_{max} has units of seconds). All of our calculations assumed $g_{max} = 10^{-14}$ s ($\Delta\tilde{\nu}_{f0}^{fwhm} \approx 3000$ cm^{-1}).

Equations 1 and 2 can be used to estimate polarization ratios by simply inserting the values of a and b appropriate for circular and parallel polarization and taking the ratio. This exercise generates the following equation for type I

$$\Omega^{I} = \frac{\cos^2 \theta_{RR} + 3}{4 \cos^2 \theta_{RR} + 2} \quad (4)$$

and type II

$$\Omega^{II} = \frac{\cos^2 \varphi_{R\Delta\mu} + 3}{4 \cos^2 \varphi_{R\Delta\mu} + 2} \quad (5)$$

processes, where the angles are defined as in eqs 1 and 2. For the sake of argument, we will assume that the two-photon properties of the $^1A_g{}^{*-}$-like state are dominated by type I processes (eqs 1 and 4) and those of the $^1B_u{}^{*+}$-like state are dominated by type II processes (eqs 2 and 5). The polarization ratios provide insight into the symmetries of the final states and can help delineate excited state manifolds. In the following discussion, we make the assumption that the only conformation of importance for peridinin in both PCP and in CS_2 solution is the all-trans chromophore shown in Figure 1. This conformation is experimentally observed for all of the chromophore sites in PCP.[13] The experimental and theoretical solvent effect study we present in a later section of this paper provides strong evidence to support an all-trans chromophore in CS_2. In fact, we selected CS_2 as the solvent in part because it provided preferential stabilization of the all-trans conformer.

The polarization ratio for peridinin in CS_2 in the two-photon absorption region between 570 and 630 nm is observed to be 0.94 ± 0.07 (Figure 5A). This is the region occupied by the upper vibronic levels of the lowest-lying $^1A_g{}^{*-}$-like state based on an analysis of the mirrored fluorescence spectrum. Explicit calculations of the angle between the two transition lengths in eq 1 for all-trans peridinin based on MNDO−PSDCI methods predicts $\theta_{RR} \approx 60°$, which gives $\Omega^{I} \approx 1.1$. Hence, we can conclude that the observed polarization data are consistent with a lowest-lying $^1A_g{}^{*-}$-like state.

The second polarization region extends from 460 to 560 nm and yields an average polarization ratio of 0.75 ± 0.09. This region is dominated by the second excited $^1B_u{}^{*+}$-like state which has the strongest two-photon absorptivity of the low-lying states. The two-photon absorptivity of the $^1B_u{}^{*+}$-like state is dominated by type II processes, and to a first approximation, the polarization ratio will be determined by $\varphi_{R\Delta\mu}$, the angle between the transition length between the ground state and the $^1B_u{}^{*+}$-like state and the vector change in dipole moment upon excitation into the same state. MNDO−PSDCI theory predicts $\varphi_{R\Delta\mu} \approx 46°$ which gives $\Omega(^1B_u{}^{*+}) \approx 0.88$. This value is higher than the observed average of $\Omega = 0.75 \pm 0.09$ but, given the single intermediate state approximation, in good agreement.

The most interesting result is the presence of a third polarization region to the blue of 460 nm. The observed polarization ratio of $\Omega \approx 1.06 \pm 0.11$ is larger than that observed in any other region and can only be explained by invoking the presence of a third excited singlet state with a small two-photon absorptivity but a large polarization ratio. We conclude that there is a third excited singlet state in this region with a vibronic peak near 450 nm. Assignment of this state cannot be made with confidence without reference to the theoretical calculations presented in the next section, where we will argue that it is a $B_u{}^{*-}$-like state.

MNDO−PSDCI Calculations on Peridinin. The effect of conformation and PCP protein environment on the excited-state properties of peridinin is presented in Figure 7, and the two-photon properties of the lowest three singlet states for selected conformers are listed in Table 1. The ground-state geometries were calculated for the vacuum conditions by using density functional methods (B3LYP) and a 6-31G(d) basis set.[52] In the case of the protein binding sites, MOPAC2000 with MOZYME linearlization were used to minimize the geometry of the chromophore within the binding site while locking all of the protein atoms. Because of the water molecules within the protein, we used the PM3 Hamiltonian, which handles discrete water molecules with greater accuracy than AM1 methods.

The first goal of this section is to complete the analysis of the two-photon excitation and polarization spectra of peridinin in CS_2. The MNDO−PSDCI calculations predict three low-

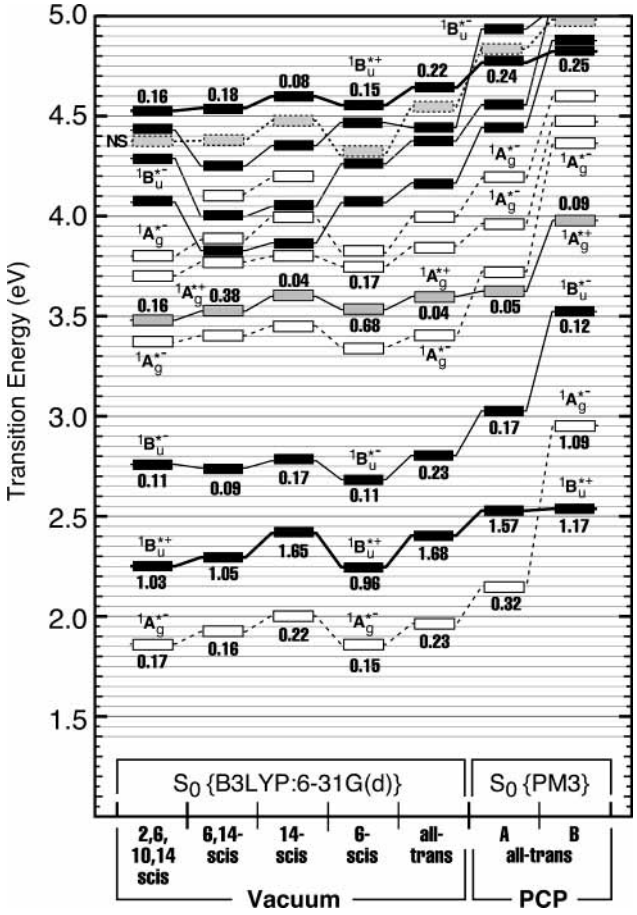

Figure 7. MNDO−PSDCI analysis of the low-lying excited singlet states of peridinin in a vacuum and in the PCP protein. The vacuum calculations used density functional methods [B3LYP/6-31G(d)] to minimize the all-trans (all-s-trans) geometry as well as for selected s-cis geometries. The calculations for PCP were carried out using a linearized SCF Hamiltonian (MOZYME in Mopac2000). The results for the extremes are shown in A and B (see text).

lying excited singlet states: S_1 is an $^1A_g{}^{*-}$-like state, S_2 is a $^1B_u{}^{*+}$-like state and S_3 is a $^1B_u{}^{*-}$-like state. The configurational properties of these three states are described in Figure 8. The first two excited singlet states display most of the characteristics that have been observed in other long-chain polyenes (see Introduction). However, the MNDO−PSDCI calculations predict one dramatic exception. The lowest-lying $^1A_g{}^{*-}$-like state is not a typical "covalent" state exhibiting dipolar properties similar to the ground state but rather a charge-transfer state exhibiting a very large change in dipole moment upon excitation (Figure 8, Table 1). The charge-transfer character of the $^1A_g{}^{*-}$-like state is important in understanding the photophysical properties of peridinin in polar solvent (see below). The configurational origin of the large change in dipole moment upon excitation derives from the significant participation of π-molecular orbitals $|8>$ (*homo*-1) and $|11>$ (*lumo*+1) (the molecular orbitals are shown in the upper left panel of Figure 8), and the way in which these orbitals are mixed into the more dominant homo and lumo contributions. The molecular origin of charge-transfer character in the "covalent" $^1A_g{}^{*-}$-like state can be traced to the orientation of the conjugated carbonyl group, which creates a local (lactone ring) dipole moment that is oriented roughly 60° from the long axis of the polyene chain. The lowest-lying $^1A_g{}^{*-}$-like state retains the low oscillator strength that is associated with a state with a high percentage of doubly excited character (48%). The strongly allowed $^1B_u{}^{*+}$-like state has much less doubly excited character (21%). However, a comparison of these numbers with the comparable percentages calculated for the long-chain, nonpolar carotenoid rhodopin glucoside[56] {$^1A_g{}^{*-}$-like state (78%D), $^1B_u{}^{*+}$-like state (6%D)}, indicates that there is considerable mixing of the low-lying $^1A_g{}^{*-}$-like and $^1B_u{}^{*+}$-like states in peridinin. This mixing can be appreciated from an observation of the large number of shared configurations for these two states as shown in Figure 8. The two-photon absorptivity of the $^1B_u{}^{*+}$-like state is calculated to be roughly 20-times larger than that calculated for the $^1A_g{}^{*-}$-like state (Table 1). Nevertheless, we believe the weak vibronic bands observed at ∼19.2, ∼18.1, and ∼17 kK in the two-photon excitation spectrum (Figure 3A) are associated with the $^1A_g{}^{*-}$-like state. The relative intensity of these bands is consistent with the calculated relative two-photon absorptivities. As we have discussed previously, the presence of the $^1A_g{}^{*-}$-like and $^1B_u{}^{*+}$-like states is clearly reflected in the two-photon polarization data shown in Figure 5 and discussed in the previous section.

This ratio is larger than that predicted by the single intermediate state approximation (eqs 1 and 2) and is due to significant contributions to the $^1B_u{}^{*+}$-like state absorptivity from other excited singlet states within the perturbation expansion. The single intermediate state approximation is not adequate for describing the absolute two-photon absorptivity of either the $^1A_g{}^{*-}$-like or $^1B_u{}^{*+}$-like states. In contrast, this approximation does a much better job of predicting the polarization ratios (see above).

The MNDO−PSDCI calculations predict that the third excited $^1B_u{}^{*-}$-like state should have an observable two-photon absorptivity, roughly comparable to that of the lowest-lying $^1A_g{}^{*-}$-like state. However, we found no evidence of the $^1B_u{}^{*-}$-like state in the two-photon excitation spectrum (Figure 3). As can be seen in Figure 5, there is a significant increase in the polarization ratio observed at 460 nm (∼2.7 eV, ∼21.8 kK) in good agreement with the calculated transition energy (2.8 eV, 22.6 kK) of the $^1B_u{}^{*-}$-like state (Table 1). Moreover, the observed polarization ratio $\Omega_{obsv} \approx 1.06$ (Figure 5) is in reasonable agreement with the calculated value of $\Omega_{calc} \approx 1.00$ (Table 1). We conclude that the polarization ratio data provide strong evidence for a third-excited $^1B_u{}^{*-}$-like state just slight above the strongly allowed $^1B_u{}^{*+}$-like state.

MNDO−PSDCI Calculations on PCP. A single monomeric unit of the PCP trimer is shown in Figure 1A. There is a pseudo-axis of symmetry that runs vertically through the center of the protein, and the peridinin molecules have been colored to reflect the symmetry relationships and are numbered following the convention used in the crystal structure analysis.[13] The crystal structure indicates that the eight peridinin binding sites are not equivalent with respect to carotenoid geometry as shown in Figure 1B. Indeed, sites 612 and 622 (colored orange in Figure 1A) are distorted relative to the other six sites. The question we sought to answer was what impact this distortion might have on the one-photon and two-photon properties of the carotenoid. Although it would be far preferable to use the crystal structure coordinates for calculating the electronic properties, such calculations are not possible unless the coordinates have been determined to sub-angstrom resolution. This limitation is associated with the extreme sensitivity of molecular orbital calculations to small changes in bond lengths and bond angles. A reasonable solution to this problem is to minimize the geometry of the carotenoid within the protein environment using molecular orbital theory. Our methods and procedures of carrying out chromophore minimizations inside protein binding sites have been discussed previously.[56,75] In the present instance,

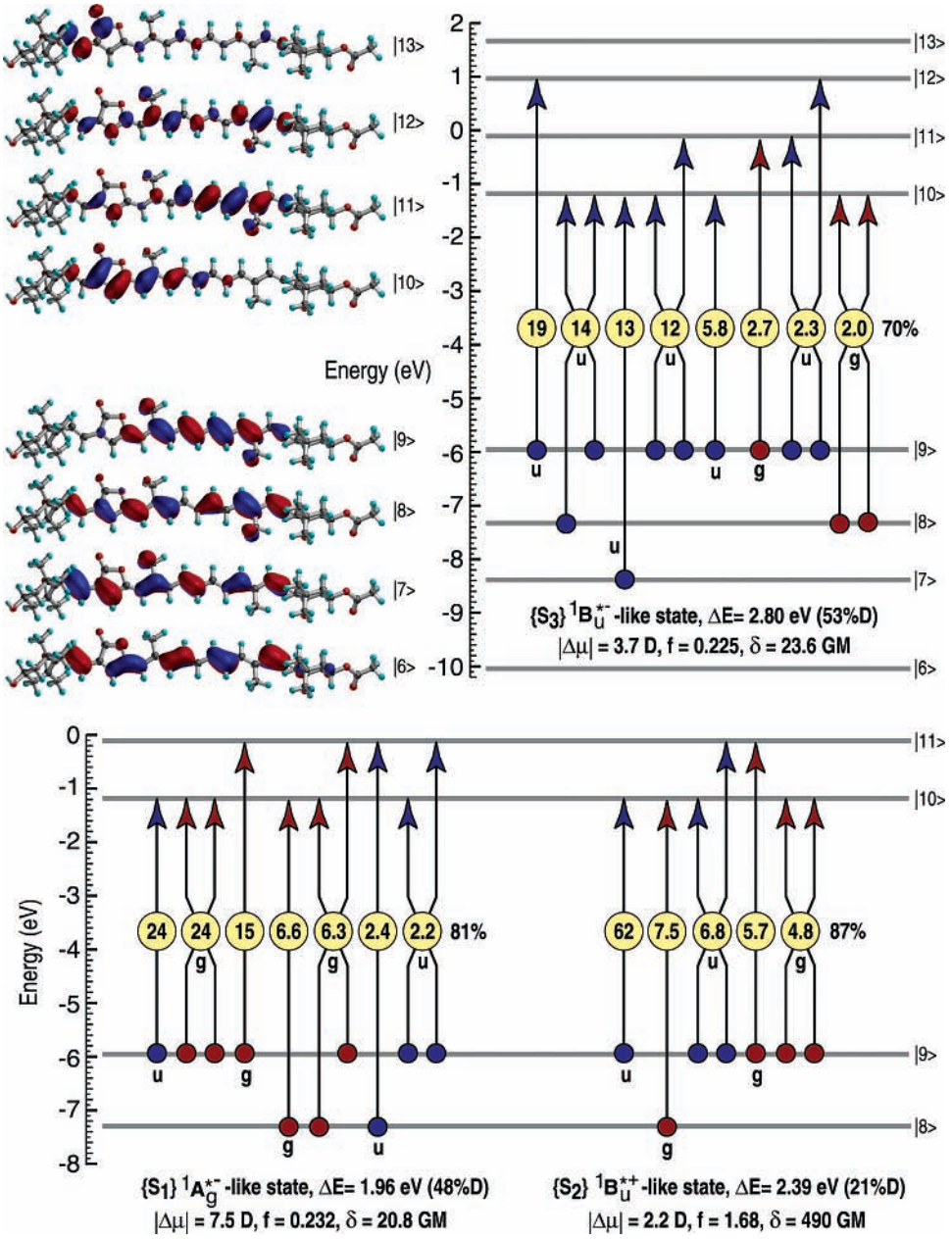

Figure 8. Configurational analysis of the three lowest-lying excited singlet states of all-trans peridinin based on MNDO−PSDCI molecular orbital theory. Each excited state is described as a linear combination of single or double excitations with the percent contribution of each configuration shown in the yellow circle. Only configurations contributing 2% or more are shown. Configurations with gerade-like symmetry are labeled "g" and are shown in red, and those with ungerade-like symmetry are labeled "u" and are shown in blue. Doubly excited configurations have two source (hole circles) and destination (particle arrows) symbols. Both S_1 ($^1A_g{}^{*-}$-like) and S_3 ($^1B_u{}^{*-}$-like) states have significant doubly excited character (48% and 53%, respectively). These states cannot be described adequately using single-CI methods. Note that S_1 and S_2 are highly mixed and share a significant number of common configurations. The wave functions of the π-electron orbitals are shown in the inset at upper left.

we used Cache 5.0 to add hydrogen atoms and Mopac2000 and the PM3 Hamiltonian to minimize all of the hydrogen atoms simultaneously. We then locked all atoms other than those associated with the chromophores and reminimized the peridinin molecules within the binding sites. The MNDO−PSDCI calculations on the minimized geometries indicated that most of the chromophores had excited state properties similar to those observed for the isolated all-trans chromophore but slightly blue shifted in terms of transition energies (see Figure 7, PCP A set for a median example). The blue shift is associated in part with distortion around the polyene single bonds, which destabilize the excited states more than the ground states due to partial bond order reversal upon excitation. However, the chromophores occupying sites 612 and 622 (orange in Figure 1) were not only blue shifted but had inverted S_1 and S_2 singlet states as shown in Figure 7, PCP B set. We find this result of considerable interest in light of the recent theoretical study by Damjanovic et al. in which the PER612 site was predicted to play a unique role in energy transfer within PCP.[21] In particular, the carotenoids occupying sites 612 and 622 were predicted to transfer their excitation energy not to the chlorophylls but to nearby peridinin molecules which serve as intermediaries with ultimate transfer to the chlorophylls. The above results suggest that the biological relevance of the level ordering reversal for PER612 and PER622 is enhanced energy transfer from these chromophores to the nearby peridinin chromophores, all of which have lower excited-state singlet levels. We note that the $^1B_u{}^{*+}$-like state provides optimal dipolar energy transfer coupling to

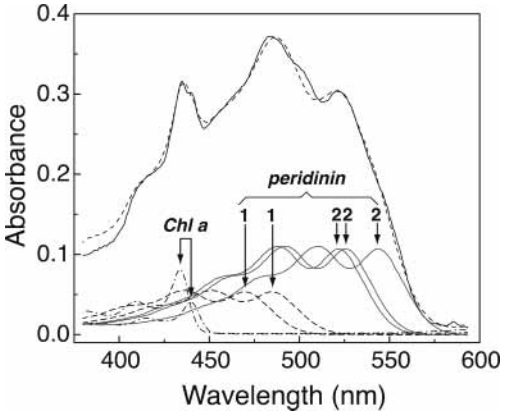

Figure 9. Analysis of the 10 K experimental absorption spectrum (solid line) of the PCP complex in the Soret and peridinin absorption regions by summation of the spectra of Chl (dashed/dotted) and peridinin (solid line and dashed) components. The absorption spectrum of the PCP complex taken in a buffer/glycerol glass at 10 K is seen in the figure to be approximated by the summation of the arbitrarily shifted absorption spectra of two Chl *a* species and eight peridinin molecules taken in 2-MTHF at the same temperature. The peridinin spectra labeled 1 are based on a single peridinin molecule, whereas those labeled 2 represent two peridinin molecules assumed to have identical electronic absorption spectra. The peak maxima in the Soret region of the two Chl *a* molecules are 433 ± 1 nm and 439 ± 1 nm.

the other peridinin molecules as discussed in Damjanovic et al.[21] Thus, the PER612 and PER622 sites optimize energy transfer by increasing $^1B_u{}^{*+}$-like state population, as this state is now the lowest excited singlet state.

The two-photon spectrum of PCP displays modest vibronic structure, and some of the bands on the red edge of the excitation profile may be associated with $^1A_g{}^{*-}$-like state contributions. However, the polarization ratio data shown in Figure 5b indicates that Ω is decreasing in the region of the first vibronic band and suggests that all of the vibronic peaks in the TPE spectrum of PCP are due to $^1B_u{}^{*+}$-like state contributions. We conclude that both the one-photon and two-photon profiles are both dominated by the peridinin $^1B_u{}^{*+}$-like states and that the differences in vibronic band maxima reflect the four different sites and differences in the electric fields within the protein. Small changes in the ground and $^1B_u{}^{*+}$-like excited-state dipole moments due to protein binding site differences would be sufficient to alter the vibronic profile of the two-photon excitation spectrum.

The two-photon excitation spectra neither support nor contradict our prediction that two of the peridinin molecules have a blue-shifted, S_1/S_2 inverted excited-state manifold. We therefore investigated this theoretical prediction by collecting the spectrum of PCP in buffer/glycerol glass at 10 K and fitting the overall spectrum to a linear combination of component spectra. Individual spectra of Chl *a* and peridinin in 2-MTHF solution at 10 K served as the component spectra, and we assumed that only the two Chl *a* and eight peridinin molecules contribute to the PCP spectrum above 375 nm. We allowed the Chl *a* components to have any intensity but locked all of the peridinin components to have the same intensity maximum. The best fit is shown in Figure 9.

The fit of the component spectra to the observed PCP spectrum is not perfect, but the general absorption profile is unique and simulated to good precision. The fit requires that the two Chl *a* spectra have different intensities, a result we attribute to exciton coupling.[25] However, the key observation is the fact that the simulation predicts two peridinin molecules (spectral origins marked with "1" in Figure 9) that are blue shifted significantly relative to the other six, which are simulated as pairs (spectral origins marked with "2" in Figure 9).

Our experimental and theoretical results are therefore consistent with a model of two peridinin molecules that are blue-shifted, and may have inverted excited singlet states. The calculations suggest these two peridinin molecules occupy sites 612 and 622 within the PCP protein (Figure 1), and on the basis of the previous theoretical studies of Damjanovic et al.,[21] we conclude that the primary biological function of these two peridinin molecules is to transfer excitation energy to the other six peridinin molecules.

Effect of Solvent Environment on Peridinin Conformation. Changes in solvent environment have a significant impact on the photophysical properties of peridinin.[20,29,30,48] There are three potential mechanisms that must be evaluated to properly understand the role that solvent can play in mediating photophysics. First, the solvent can preferentially select conformers that have different ground and excited state properties. Second, the solvent can induce a reaction field that reorganizes the electronic structure and alter the excited state level ordering or mixing. Third, a solvent can couple directly with the solute and alter the photophysical properties via covalent or ionic interactions. All three of these interactions can be considered a logical possibility for peridinin, and we will investigate all three in the following sections.

Our first goal is to determine whether peridinin changes conformation in response to changes in solvent environment. We carried out a conformational search using MOPAC 2000 to find the lowest energy conformer in both vacuum and in water. We selected water as the polar solvent because both COSMO[64] and MST[65,66] methods have been parametrized for water. We minimized all possible single bond isomers using COSMO/AM1 methods, and used these results to search for multi-s-cis conformers that might have lower energy. The lowest energy conformers were then also examined by using density functional methods (B3LYP) and a 6-31G(d) basis set. We analyze the ground-state properties of the three lowest energy conformers in Figure 10.

The conformation shown in Figure 10A is the all-trans conformer which is identical to the conformation found in the PCP binding sites (Figure 1). Density functional methods predict that the all-trans conformer is the most stable in a vacuum, whereas the semiempirical methods predict the 14-s-cis conformer (Figure 10B) is slightly more stable (see below). The all-trans conformer is calculated to have the highest polarizability, which leads to the prediction that highly dispersive solvents (such as CS_2) will preferentially stabilize the all-trans conformer. The 14-s-cis conformer shown in Figure 10B has a comparable energy and may be populated in both polar and nonpolar solvent environments (see discussion below). More interestingly, we have found a multi-s-cis conformer that is predicted by both AM1/COSMO and AM1/MST methods to have a lower energy than the all-trans conformer in water (Figure 10C). This conformer has four s-cis bonds at atom positions 2, 6, 10, and 14 and is preferentially stabilized in polar media because it has a smaller cavity but a larger dipole moment (Figure 10). This conformer is predicted to be the most stable conformer in water, and this prediction is true for AM1, PM3, and PM5 Hamiltonians. The density functional calculations predict that the all-trans conformer is 10 kcal/mol (42 kJ/mol) lower in energy than the multi-cis conformer in a vacuum, and this difference is significantly larger than the solvent stabilization associated with the multi-cis geometry. Given the lack of

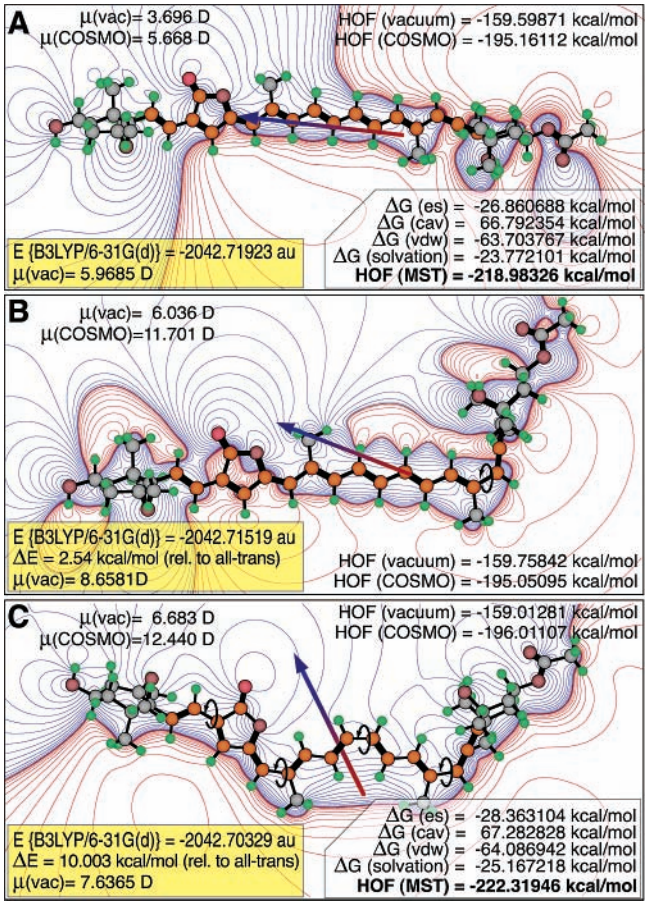

Figure 10. Energetic and dipolar properties of all-trans (A), 14-s-cis (B), and 2,6,10,14-s-cis (C) peridinin. The structures and dipole directions (red-blue arrows, red end positive) are based on density functional methods (B3LYP/6-31G(d)) and the vacuum energies and dipole moments are shown in yellow rectangles in the lower left corner of each figure section. All other data are from AM1 semiempirical calculations for vacuum or water (COSMO minimization and MST solvation analyses, see text). The MST calculations did not converge for 14-s-cis. The semiempirical SCF calculations predict that the 14-s-cis geometry (B) is the most stable in a vacuum but that the 2,6,10,14-s-cis conformation (C) is the most stable in water. In contrast, density functional methods (B3LYP/6-31G(d)) predict that the all-trans conformer is the most stable in both vacuum and water although the 14-s-cis conformer (B) has an energy difference sufficiently small relative to the all-trans conformer that both may be populated at room temperature (see text).

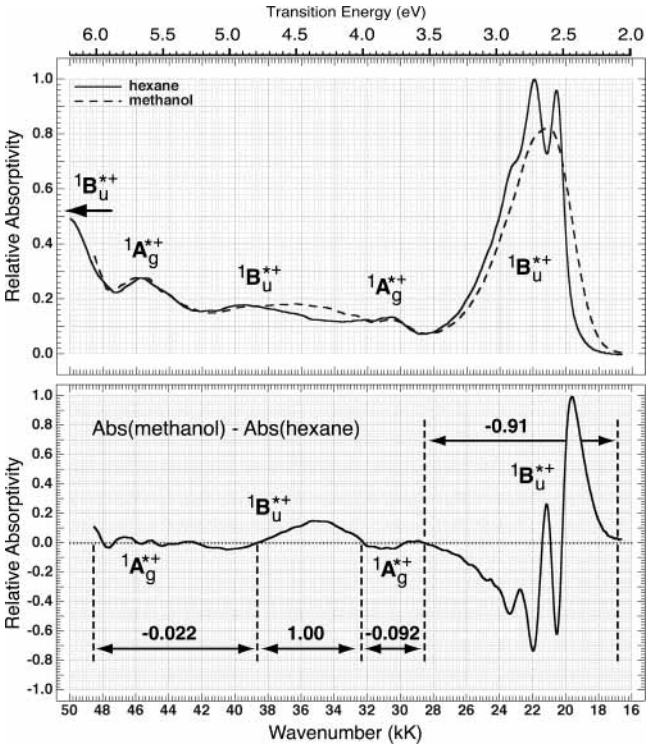

Figure 11. Effect of solvent environment on the higher energy absorption bands of peridinin in hexane and methanol. The lower difference spectrum ($A_{\text{methanol}} - A_{\text{hexane}}$) is marked off into regions for which the relative change in oscillator strength is calculated based on the integral under the curve. The allowed bands are assigned based on the MNDO−PSDCI calculations.

agreement, we examined the role of solvent on conformer stability experimentally.

The absorption spectra of peridinin in hexane and methanol at room temperature are shown in Figure 11. The difference spectrum was generated and shown in the bottom graph, with selected regions analyzed with respect to relative change in oscillator strength. We used the results of the calculations presented in Figure 10 and the MNDO−PSDCI calculations shown in Figure 7 to interpret the spectra. The principal findings are summarized in Figure 12. The semiempirical ground state calculations shown in Figure 10 indicate that the 14-s-cis conformer is the most stable in a vacuum, whereas the density functional methods predict the all-trans conformer is the most stable. Both calculations are in agreement that these two conformers are very close in energy, and we postulate that in hydrocarbon solvent both species are populated. The COSMO calculations suggest that the all-trans conformer is preferentially stabilized in polar solvent, a surprising result given the observation that the 14-s-cis has a larger dipole moment. However, the total dipole moment of this complex molecule is made up of contributions from four separate regions of the molecule, and the total dipole moment is less important than local stabilization effects. Based on a systematic analysis of the simulated spectra, we conclude that both the 14-s-cis and all-trans conformers are populated in hexane solution and that the all-trans conformer is preferentially populated in methanol.

We show two simulated difference spectra in Figure 12A. The solid line is generated by subtracting the calculated spectrum of all-trans peridinin from the calculated spectrum of all-trans peridinin plus 24 water molecules. To compare the calculated and observed difference spectra, we use a simple integral approach to analyze the shift in band intensities. The integral under a relative absorptivity difference versus wavenumber curve is proportional to the change in oscillator strength for the region of interest. Three regions are identified in Figure 12A, and the relative integrals are listed above the spectrum assigning the central difference band at 32 000 cm^{-1} to have an integral of 1. The experimental data shown in Figure 11 (bottom) is to be compared to the calculated results in Figure 12A. Integral comparisons are valuable because MNDO−PSDCI theory is more accurate in calculating the intensity of an absorption band than in predicting the transition energy. The dashed line is generated by subtracting the calculated spectrum of 14-s-cis peridinin from the calculated spectrum of all-trans peridinin plus 24 water molecules. The comparable integrals are listed below and delineated with dashed vertical lines. No combination of theoretical spectra provides perfect agreement with the observed difference spectrum (Figure 11), but our use of semiempirical MNDO−PSDCI procedures and water, instead of methanol, would make any close agreement fortuitous.

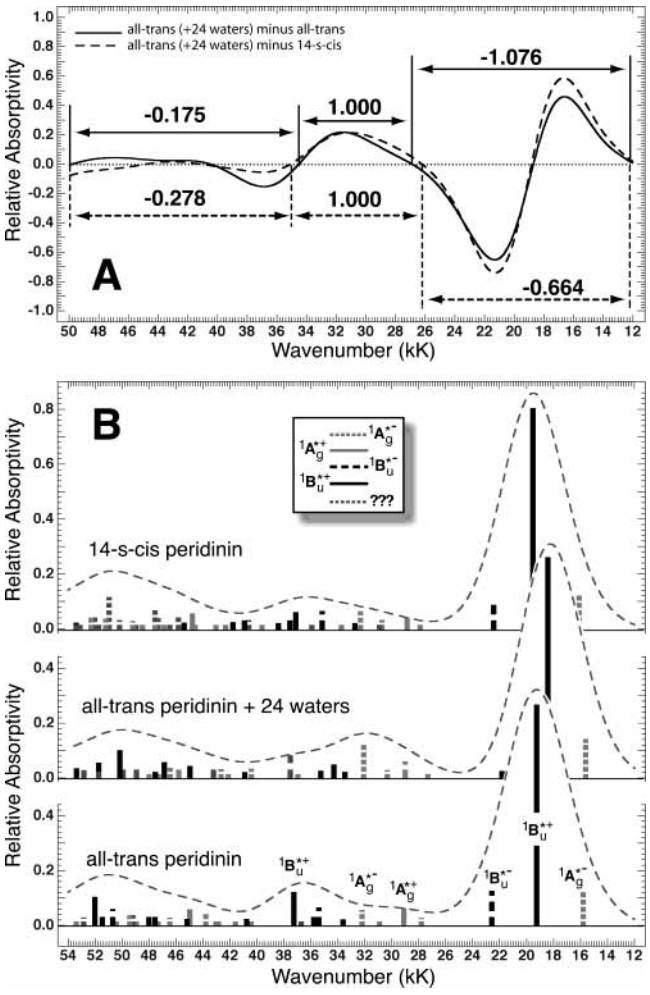

Figure 12. Simulation of the effect of polar solvent on the absorption spectrum of peridinin based on MNDO−PSDCI calculations on all-trans peridinin and 14-s-cis peridinin. The spectra at top (A) were generated by subtracting the simulated spectrum of all-trans (solid line) or 14-s-cis (dashed line) peridinin from the simulated spectrum of all-trans peridinin plus 24 water molecules. These should be compared with the experimental difference spectrum shown in Figure 11. The simulated spectra of the individual conformers are shown in (B) with the transitions shown using vertical lines with the height proportional to oscillator strength and the line-type indicating the approximate symmetry of the excitation (see insert in B).

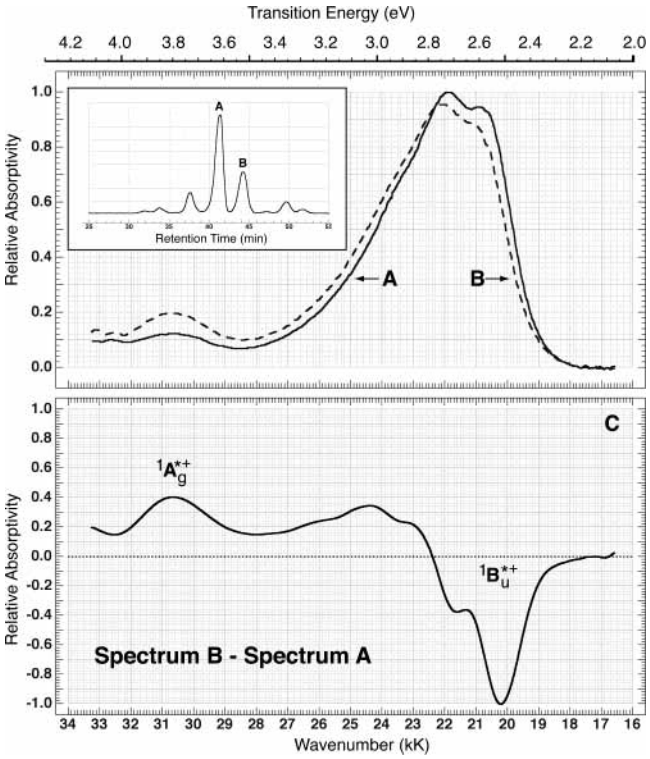

Figure 13. Absorption spectra of (A) *trans*- and (B) *cis*-peridinin isomers taken at room temperature. The inset shows the HPLC profile of peridinin obtained by separation on a 5μ Techsphere nitrile column employing a mobile phase of 89:10:1 v/v hexane−acetone−methanol at a flow rate of 1 mL/min which demonstrates baseline separation of the geometric isomers. Spectrum C shown at the bottom is the difference between spectra B and A. This figure was adapted from data provided by Synnøve Liaaen-Jensen (personal communication) following the analysis described for peridinin cis isomers given in the paper by Haugan et al. [*Acta Chem. Scand.* **1994**, *48*, 769−779].

Nevertheless, the simulation in Figure 12 provides good evidence to suggest that some 14-s-cis conformer is present in ambient temperature hexane solution and that the amount of the all-trans conformer is increased in methanol. Simulations based on increasing the amount of 14-s-cis in methanol were generated and failed significantly. If we allow for fractional mixtures, the best fit is obtained by assuming that the methanol spectrum is pure all-trans but that the hexane solution is a mixture of 75% all-trans and 25% 14-s-cis. Our spectral simulations found no evidence of the multicis conformer shown in Figure 10C and predicted by the semiempirical calculations to be the lowest energy conformer in polar solvent.

When we first measured the methanol minus hexane difference spectrum shown in Figure 11, we considered the possibility that the strong positive band at ∼35 000 cm^{-1} might be due to a cis band. These bands are associated with $^1A_g{}^{*+}$-like states and are used as a spectroscopic diagnostic of single or double bond cis conformations.[76,77] However, the MNDO−PSDCI calculations predict that the cis band is located at about ∼29 000 cm^{-1} in peridinin, much lower in energy than the ∼35 000 cm^{-1} difference band. We sought confirmation of this assignment by examining the difference spectrum of a known cis isomer, and the results are shown in Figure 13. As can be seen in this figure, the cis band is observed at ∼30 800 cm^{-1}, in reasonable agreement with the MNDO−PSDCI calculations. Thus, both theory and experiment support our general conclusion that methanol solvent preferentially stabilizes the all-trans conformer.

Effect of Solvent Environment on Peridinin Photophysics. The effect of solvent environment on the absorption and fluorescence spectra of peridinin is summarized in Figure 14. The most important observation is the relative energy shift in the absorption maxima versus emission maxima in going from a nonpolar solvent [hexane (n = 1.3723, ϵ = 1.880, 25 °C)] to a highly polar solvent [acetonitrile (n = 1.3415, ϵ = 36.5, 25 °C)]. The key observation is that the red shift observed in the strongly allowed λ_{max} absorption band is much smaller that of the corresponding red shift observed in the fluorescence maximum. This observation has important implications with respect to the dipole moments of the S_1 and S_2 excited singlet states.

The shift in the absorption spectrum due to first-order dipolar reaction field effects can be estimated by the equation[78]

$$\Delta\tilde{\nu}_{abs} = \frac{2}{hc}\frac{\mu_{00}(\mu_{00} - \mu_{bb})}{a^3} f_{solv} \qquad (6)$$

where μ_{00} is the ground-state dipole moment, μ_{bb} is the dipole moment of the state responsible for the absorption band, a is

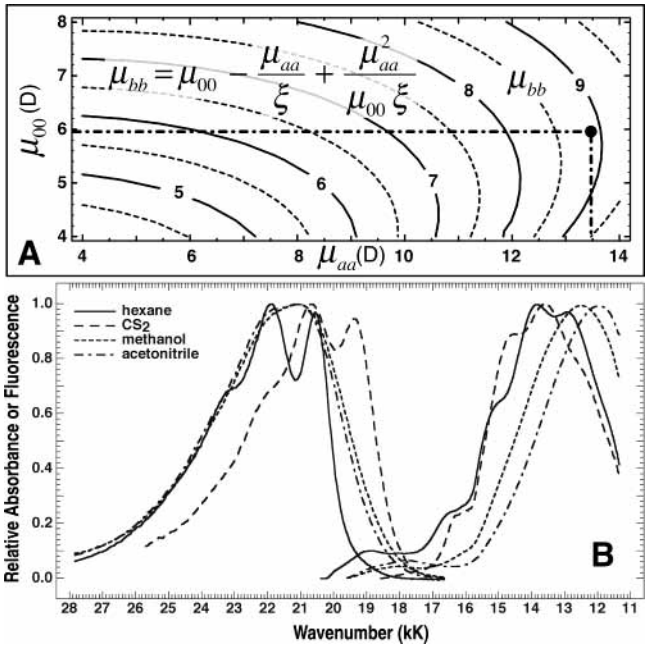

Figure 14. Effect of solvent environment on the absorption and fluorescence spectra of peridinin (B) and contours of the S_2,$^1B_u{}^{*+}$-like state dipole moment, μ_{bb}, as a function of the ground (μ_{00}) and S_1, $^1A_g{}^{*-}$-like excited singlet state (μ_{aa}) dipole moments (A). The spectra in B were collected in four different solvents that provide four unique solvent environments: hexane (nonpolar), carbon disulfide (nonpolar, dispersive), acetonitrile (polar), and methanol (polar, hydrogen bonding). Note that the influence of solvent environment on the absorption and emission spectra is significantly different, which is consistent with the fact that the emitting [S_1 ($^1A_g{}^{*-}$-like)] and absorbing [S_2 ($^1B_u{}^{*+}$-like)] states are different. The contour map in A was generated assuming that $\xi = \Delta\tilde{\nu}_{fluor}/\Delta\tilde{\nu}_{abs} = 5.8$ (eq 9).

the solute cavity radius and f_{solv} is the solvent reaction field parameter given by

$$f_{solv} = \frac{\epsilon - 1}{\epsilon + 2} - \frac{n^2 - 1}{n^2 + 2} \tag{7}$$

The shift in the fluorescence spectrum can also be calculated, and is given by[78]

$$\Delta\tilde{\nu}_{fluor} = \frac{2}{hc}\frac{\mu_{aa}(\mu_{00} - \mu_{aa})}{a^3} f_{solv} \tag{8}$$

where μ_{aa} is the dipole moment of the emitting state. Equations 6 and 9 are based on a simple spherical cavity model that neglects higher order Stark terms. However, a higher-order treatment cannot be justified because we do not have the necessary polarizability data, nor is it required for the simple ratioing method we employ below. Our goal is to generate a relationship that helps define the differences between μ_{aa} and μ_{bb}. By using hexane as a standard ($f_{solv} \approx 0$), we use the data for acetonitrile to define $\Delta\tilde{\nu}_{abs}$(21 210 − 21 430 = −220 cm^{-1}) and $\Delta\tilde{\nu}_{fluor}$ (12 030 − 13 300 = −1270 cm^{-1}), where the numbers in parentheses are the maxima in hexane minus the maxima in acetonitrile. These numbers are negative because acetonitrile causes a red shift in both the absorption (−220 cm^{-1}) and fluorescence (−1270 cm^{-1}) bands. We take the ratio of the fluorescence divided by absorption shift

$$\xi = \frac{\Delta\tilde{\nu}_{fluor}}{\Delta\tilde{\nu}_{abs}} = 5.8 \text{ (acetonitrile using hexane as reference)} \tag{9}$$

noting that this is given by eq 8 divided by eq 6

$$\mu_{bb} = \mu_{00} - \frac{\mu_{aa}}{\xi} + \frac{\mu_{aa}^2}{\mu_{00}\xi} \tag{10}$$

This equation has three unknowns, so two must be known in order to assign the remaining value. We present a contour map of the S_2,$^1B_u{}^{*+}$-like state dipole moment, μ_{bb}, as a function of the ground (μ_{00}) and S_1, $^1A_g{}^{*-}$-like excited singlet state (μ_{aa}) dipole moments in Figure 14A. The key observation is that for reasonable values of the ground (μ_{00}) and S_1, $^1A_g{}^{*-}$-like excited singlet state (μ_{aa}) dipole moments, the $^1B_u{}^{*+}$-like state dipole moment, μ_{bb}, always has a value greater than the ground-state dipole moment but much less than μ_{aa}. The most accurate value we have for the ground-state dipole moment of all-trans peridinin is 5.97 D, which is based on the density functional calculation (B3LYP/6-31G(d), Figure 10A). If we assign this value to μ_{00} and take the change in dipole moment for the $^1A_g{}^{*-}$-like excited singlet state from Table 1 ($\Delta\mu_{a0} = \mu_{aa} - \mu_{00} = 7.5$ D), we calculate a value of 8.88D for μ_{bb}, which means a change in dipole moment of $\Delta\mu_{b0} = \mu_{bb} - \mu_{00} = 8.9 - 6.0 = 2.9$ D. The MNDO−PSDCI calculations predict $\Delta\mu_{b0} = 2.2$D (Table 1). Thus, the solvent effect calculations and the theoretical calculations are in good agreement that the change in dipole moment between the ground and the lowest-energy $^1A_g{}^{*-}$-like excited singlet state is more than two-times greater than that between the ground and the strongly allowed $^1B_u{}^{*+}$-like state. Thus, the S_1 state is indeed a charge transfer state with a dipole moment change of approximately 7.2 ± 1.4 D, where the error range includes the anticipated experimental and theoretical errors. This observation is in good agreement with recent studies.[20,29,30,48] The MNDO−PSDCI and COSMO calculations indicate that the charge-transfer character of the $^1A_g{}^{*-}$-like excited singlet state is always present and that the change in dipole moment upon excitation is nearly invariant to the solvent reaction field. The ground-state dipole moment is enhanced by a polar reaction field, and we conclude that some of the studies that have suggested an increase in the charge-transfer character of S_1 with solvent polarity are based on experiments that are more sensitive to $\Delta\mu_{a0}\mu_{00} = (\mu_{aa} - \mu_{00})\mu_{00}$ than just $\Delta\mu_{a0}$.[20,29,30,48]

Discrete Solvent Effects and Hydrogen Bonding. To investigate the effect of discrete solvent interactions and hydrogen bonding on the photophysical properties of peridinin, we added individual water molecules to peridinin and minimized these discrete molecules using MM2 mechanics followed by density functional (1−3 waters) or PM3 semiempirical (24 waters) methods. The results are shown in Table 2. The first water molecule hydrogen bonds to the carbonyl oxygen of the lactone ring, and we can use the results for this discrete interaction calculation to estimate the impact of hydrogen bonding on the photophysical properties. Examination of Table 2 indicates that hydrogen bonding induces a red shift in all three of the low-lying singlet transitions. As more water molecules are added, the$^1A_g{}^{*-}$-like excited singlet state blue shifts while the other states stay at roughly the same energy. Discrete water causes a significant decrease in the oscillator strength of the $^1B_u{}^{*-}$-like state, with a concomitant transfer of oscillator strength to the $^1A_g{}^{*-}$-like and $^1B_u{}^{*+}$-like excited singlet states. Note that these three states have a summed oscillator strength of 2.14 in a vacuum and a summed oscillator strength of 2.04 with 24 water molecules. The loss of 0.1 in the summed oscillator strengths is due to hydrogen bonding, and it is evident upon addition of a single water molecule (Table 1).

Although much remains to be fully explored, these simple theoretical studies provide a perspective on the role of solvent

TABLE 2: Effect of Discrete Solvent Molecules on *all-trans*-Peridinin Based on MNDO-PSDCI Calculations[a]

			ΔE		$\langle A \rangle$	$\langle B \rangle$	$\langle C \rangle$	$\langle D \rangle$		$\Delta\mu$	$\Delta\alpha$	DCI
solvent	S_n	sym	eV	f	GM	GM	GM	GM	Ω	D	Å^3	%
vacuum	S_1	A_g^-	1.96	0.23	20.79	11.62	23.24	9.17	1.12	7.49	51.60	48
	S_2	B_u^+	2.39	1.68	489.97	219.46	438.92	270.51	0.90	2.16	179.10	21
	S_3	B_u^-	2.80	0.23	23.57	11.82	23.63	11.75	1.00	3.69	27.00	53
H_2O	S_1	A_g^-	1.90	0.22	44.47	13.93	27.87	30.54	0.63	6.03	53.96	48
	S_2	B_u^+	2.34	1.69	823.61	268.13	536.26	554.48	0.65	3.36	183.46	21
	S_3	B_u^-	2.70	0.15	166.18	21.26	42.52	144.92	0.26	2.05	21.90	56
3(H_2O)	S_1	A_g^-	1.88	0.24	51.99	17.21	34.41	34.78	0.66	4.93	61.15	46
	S_2	B_u^+	2.30	1.71	795.77	275.23	550.47	520.54	0.69	2.21	182.58	22
	S_3	B_u^-	2.68	0.07	40.84	cf[b]	cf[b]	cf[b]	cf[b]	1.26	16.44	58
24(H_2O)	S_1	A_g^-	1.94	0.27	78.37	24.10	48.21	54.27	0.62	7.95	74.56	44
	S_2	B_u^+	2.29	1.76	2306.7	767.60	1535.3	1539.0	0.66	7.54	183.05	23
	S_3	B_u^-	2.71	0.01	28.83	9.19	18.39	19.64	0.26	1.01	10.68	59

[a] The ground-state geometry was calculated using Gaussian 98 and density functional methods [B3LYP/6-31G(d)]. In calculations using three or less solvent molecules, the solvent molecules were also minimized using the same density functional methods. Higher solvent ensembles were minimized using PM3 methods. The first column gives the discrete solvent system and the remaining columns are defined as in Table 1. [b] cf indicates that the calculation failed either because the perturbation calculation did not converge or a false resonance made the result unreliable.

in mediating the photophysical properties of peridinin in solution. A polar solvent environment increases the oscillator strength of the lowest-lying $^1A_g{}^{*-}$-like excited singlet state and enhances both radiative and nonradiative coupling of this state into the ground state. Hydrogen bonding enhances this coupling, but any polar solvent will decrease the lifetime of the excited singlet state manifold.

Comments and Conclusions

The large ground-state dipole moment of all-trans peridinin (~6 D in nonpolar solvent, ~10 D in polar solvent, Figure 10A), and the fact that the conjugated lactone ring generates an off-axis electrostatic field, generates unique photophysical properties of the low-lying singlet state manifold. An analysis of the two-photon excitation and polarization data (Figures 3 and 5) and the fluorescence data (Figure 3) reveals three low-lying excited singlet states: a $^1A_g{}^{*-}$-like state with a system origin at ~16 200 cm^{-1}, a $^1B_u{}^{*+}$-like state with a system origin at ~19 300 cm^{-1} and a $^1B_u{}^{*-}$-like state with a system origin at ~22 000 cm^{-1} in CS_2. The two-photon excitation spectrum shows additional vibronic maxima of the $^1A_g{}^{*-}$-like state as weak features at ~19.2, ~18.1, and ~17 kK (Figure 3). MNDO−PSDCI theory and solvent effect studies indicate that the S_1 state has a large dipole moment (~16 D) in both polar and nonpolar environments. Thus, the $^1A_g{}^{*-}$-like state is the charge-transfer state ($\Delta\mu \approx 8$ D) observed in previous studies. The suggestion that the charge-transfer character is induced in polar solvent is not supported by our studies. We conclude that some of the studies that have suggested an increase in the charge-transfer character of S_1 with solvent polarity are based on experiments that are more sensitive to $(\mu_{aa} - \mu_{00})\mu_{00}$ than $(\mu_{aa} - \mu_{00})$, where μ_{00} is the ground-state dipole moment and μ_{aa} is the dipole moment of the lowest-lying $^1A_g{}^{*-}$-like state.[20,29,30,48]

In ambient temperature hydrocarbon solvent, peridinin exists as a mixture of all-trans (Figure 10A) and 14-s-cis (Figure 10B) conformers, with a predominance of the former. The absorption spectra of these two conformers are very similar, and only in the higher energy regions of the spectrum can one find experimentally observable differences (Figures 11 and 12). Polar solvents such as methanol and high-dielectric solvents such as CS_2 preferentially stabilize the all-trans conformer relative to the 14-s-cis. No experimental evidence was found to support the presence of a multicis conformer (Figure 10C) predicted by MOPAC COSMO and MST methods to be the most stable conformer in highly polar solvent.

MNDO−PSDCI calculations on the minimized peridinin molecules within PCP indicate that most of the chromophores have excited state properties similar to those observed for the isolated all-trans chromophore but slightly blue shifted in terms of transition energies (see Figure 7, PCP A set for a median example). However, the chromophores occupying sites 612 and 622 (orange in Figure 1) are not only blue-shifted but have inverted S_1 and S_2 singlet states as shown in Figure 7 (PCP B). Damjanovic et al. predict theoretically that the carotenoids occupying these sites transfer their excitation energy not to the chlorophylls but to nearby peridinin molecules.[21] We conclude that the PER612 and PER622 sites optimize energy transfer by increasing $^1B_u{}^{*+}$-like state population, as this state is now the lowest excited singlet state and offers better dipolar coupling to the other peridinin molecules. A fit of component spectra to the PCP complex spectrum supports the assignment of two peridinin molecules having unique, blue-shifted spectra (Figure 9).

Acknowledgment. The authors thank Eckhard Hofmann for helpful discussions regarding the peridinin binding sites in PCP, Synnøve Liaaen-Jensen for providing valuable information regarding geometric isomers of peridinin, Graham Fleming for sharing the details of his two-photon experimental observations on peridinin and the PCP complex prior to publication, and Tomás Polívka and Ronald Christensen for helpful discussions. This work was supported by grants from the National Institutes of Health (GM-34358 to RRB, GM-30353 to HAF), the National Science Foundation (EIA-0129731 to RRB, MCB-9816759 to HAF), and the University of Connecticut Research Foundation to HAF. Funding for BJS was provided by an NSF Research Experience for Undergraduates (REU) program (CHE-9732366) at the University of Connecticut.

References and Notes

(1) Blankenship, R. E.; Madigan, M. T.; Bauer, C. E. *Anoxygenic photosynthetic bacteria*; Kluwer Academic Publishers: Dordrecht, The Netherlands, 1995; Vol. 2.

(2) Song, P.-S.; Koka, P.; Prézelin, B. B.; Haxo, F. T. *Biochemistry* **1976**, *15*, 4422−4427.

(3) Koka, P.; Song, P.-S. *Biochim. Biophys. Acta* **1977**, *495*, 220−231.

(4) Mimuro, M.; Nagashima, U.; Nagaoka, S.; Nishimura, Y.; Takaichi, S.; Katoh, T.; Yamazaki, I. *Chem. Phys. Lett.* **1992**, *191*, 219−224.

(5) Mimuro, M.; Nishimura, Y.; Takaichi, S.; Yamano, Y.; Ito, M.; Nagaoka, S.; Yamazaki, I.; Katoh, T.; Nagashima, U. *Chem. Phys. Lett.* **1993**, *213*, 576−580.

(6) Ogata, T.; Kodama, M.; Nomura, S.; Kobayashi, M.; Nozawa, T.; Katoh, T.; Mimuro, M. *FEBS Lett.* **1994**, *356*, 367−371.
(7) McDermott, G.; Prince, S. M.; Freer, A. A.; Hawthornthwaite-Lawless, A. M.; Papiz, M. Z.; Cogdell, R. J.; Isaacs, N. W. *Nature (London)* **1995**, *374*, 517−521.
(8) Koepke, J.; Hu, X.; Schulten, K.; Michel, H. *Structure* **1996**, *4*, 581−597.
(9) Kühlbrandt, W.; Wang, D. N.; Fujiyoshi, Y. *Nature* **1994**, *367*, 614−621.
(10) Matthews, B. W.; Fenna, R. E.; Bolognesi, M. C.; Schmid, M. F.; Olsen, J. M. *J. Mol. Biol.* **1979**, *181*, 259−285.
(11) Hiller, R. G. Carotenoids as components of the light-harvesting proteins of eukaryotic algae. In *The Photochemistry of Carotenoids*; Frank, H. A., Young, A. J., Britton, G., Cogdell, R. J., Eds.; Kluwer Academic: Dordrecht, The Netherlands, 1999; Vol. 8, pp 81−98.
(12) Hiller, R. G.; Crossley, L. G.; Wrench, P. M.; Santucci, N.; Hofmann, E. *Mol. Genet. Genomics* **2001**, *266*, 254−259.
(13) Hofmann, E.; Wrench, P. M.; Sharples, F. P.; Hiller, R. G.; Welte, W.; Diederichs, K. *Science* **1996**, *272*, 1788−1791.
(14) Bautista, J. A.; Hiller, R. G.; Sharples, F. P.; Gosztola, D.; Wasielewski, M.; Frank, H. A. *J. Phys. Chem. A* **1999**, *103*, 2267−2273.
(15) Akimoto, S.; Takaichi, S.; Ogata, T.; Nishimura, Y.; Yamazaki, I.; Mimuro, M. *Chem. Phys. Lett.* **1996**, *260*, 147−152.
(16) Carbonera, D.; Giacometti, G.; Agostini, G. *Spectrochim. Acta* **1995**, *51A*, 115−123.
(17) Carbonera, D.; Giacometti, G.; Segre, U.; Angerhofer, A.; Gross, U. *J. Phys. Chem. B* **1999**, *103*, 6357−6362.
(18) Krueger, B. P.; Lampoura, S. S.; van Stokkum, I. H. M.; Papagiannakis, E.; Salverda, J. M.; Gradinaru, C. C.; Rutkauskas, D.; Hiller, R. G.; van Grondelle, R. *Biophys. J.* **2001**, *80*, 2843−2855.
(19) Ritz, T.; Damjanovic, A.; Schulten, K.; Zhang, J.-P.; Koyama, Y. *Photosynth. Res.* **2001**, *66*, 125−144.
(20) Zigmantas, D.; Polivka, T.; Hiller, R. G.; Yartsev, A.; Sundström, V. *J. Phys. Chem. A* **2001**, *105*, 10296−10306.
(21) Damjanovic, A.; Ritz, T.; Schulten, K. *Biophys. J.* **2000**, *79*, 1695−1705.
(22) Kleima, F. J.; Hofmann, E.; Gobets, B.; Van Stokkum, I. H. M.; Van Grondelle, R.; Van Amerongen, H. Peridinin chlorophyll protein: Structure and dynamics related. *Photosynthesis: Mechanisms and Effects*; Budapest, Hungary, 1998.
(23) Kleima, F. J.; Wendling, M.; Hofmann, E.; Peterman, E. J. G.; van Grondelle, R.; van Amerongen, H. *Biochemistry* **2000**, *39*, 5184−5195.
(24) Kleima, F. J.; Hofmann, E.; Gobets, B.; Van Stokkum, I. H. M.; Van Grondelle, R.; Diederichs, K.; Van Amerongen, H. *Biophys. J.* **2000**, *78*, 344−353.
(25) Carbonera, D.; Giacometti, G.; Segre, U. Carotenoid interactions in peridinin-chlorophyll proteins from dinoflagellates: evidence for optical excitons and triplet migration. *Photosynthesis: from Light to Biosphere*; Montpellier, France, 1995.
(26) Osaka, A.; Kume, T. *Tetrahedron Lett.* **1998**, *39*, 655−658.
(27) Pilch, M.; Pawlikowski, M. *J. Chem. Soc., Faraday Trans.* **1998**, *94*, 227−232.
(28) Iglesias-Prieto, R.; Trench, R. K. *J. Plant Physiol.* **1996**, *149*, 510−516.
(29) Bautista, J. A.; Connors, R. E.; Raju, B. B.; Hiller, R. G.; Sharples, F. P.; Gosztola, D.; Wasielewski, M. R.; Frank, H. A. *J. Phys. Chem. B* **1999**, *103*, 8751−8758.
(30) Frank, H. A.; Bautista, J. A.; Josue, J.; Pendon, Z.; Hiller, R. G.; Sharples, F. P.; Gosztola, D.; Wasielewski, M. R. *J. Phys. Chem. B* **2000**, *104*, 4569−4577.
(31) Hudson, B.; Kohler, B. *Annu. Rev. Phys. Chem.* **1974**, *25*, 437−460.
(32) Birge, R. R.; Schulten, K.; Karplus, M. *Chem. Phys. Lett.* **1975**, *31*, 451−454.
(33) Birge, R. R. *Annu. Rev. Biophys. Bioeng.* **1981**, *10*, 315−354.
(34) Birge, R.; Pierce, B. *J. Chem. Phys.* **1979**, *70*, 165−167.
(35) Birge, R. R. *Acc. Chem. Res.* **1986**, *19*, 138−146.
(36) Frank, H. A.; Chynwat, V.; Desamero, R. Z. B.; Farhoosh, R.; Erickson, J.; Bautista, J. *Pure Appl. Chem.* **1997**, *69*, 2117−2124.
(37) Sashima, T.; Koyama, Y.; Yamada, T.; Hashimoto, H. *J. Phys. Chem. B* **2000**, *104*, 5011−5019.
(38) Sashima, T.; Nagae, H.; Kuki, M.; Koyama, Y. *Chem. Phys. Lett.* **1999**, *299*, 187−194.
(39) Sashima, T.; Shiba, M.; Hashimoto, H.; Nagae, H.; Koyama, Y. *Chem. Phys. Lett.* **1998**, *290*, 36−42.
(40) Koyama, Y.; Fujii, R. Cis−trans carotenoids in photosynthesis: Configurations, excited-state properties and physiological functions. In *The Photochemistry of Carotenoids*; Frank, H. A., Young, A. J., Britton, G., Cogdell, R. J., Eds.; Kluwer Academic Publishers: Dordrecht, The Netherlands, 1999; Vol. 8, pp 161−188.
(41) Goodwin, T. W. In *Chemistry and Biochemistry of Plant Pigments*; Goodwin, T. W., Ed.; Academic Press: New York, 1976; Vol. 1, p 228.
(42) Liaaen-Jensen, S. In *Carotenoids*; Britton, G., Liaaen-Jensen, S., Pfander, H., Eds.; Birkhäuser Verlag: Berlin, 1998; Vol. 3, p 217.
(43) Johansen, J. E.; Svec, W. A.; Liaaen-Jensen, S.; Haxo, F. T. *Phytochemistry* **1974**, *12*, 2261.
(44) Liaaen-Jensen, S. In *Carotenoids*; Isler, O., Gutmann, H., Solms, U., Eds.; Birkhäuser Verlag: Basel, 1971; p 163.
(45) Mimuro, M.; Nagashima, U.; Takaichi, S.; Nishimura, Y.; Yamazaka, I.; Katoh, T. *Biochim. Biophys. Acta* **1992**, *1098*, 271−274.
(46) DeCoster, B.; Christensen, R. L.; Gebhard, R.; Lugtenburg, J.; Farhoosh, R.; Frank, H. A. *Biochim. Biophys. Acta* **1992**, *1102*, 107−114.
(47) Zigmantas, D.; Hiller, R. G.; Sundstroem, V.; Polivka, T. *Proc. Natl. Acad. Sci. U.S.A.* **2002**, in press.
(48) Zigmantas, D.; Hiller, R. G.; Yartsev, A.; Sundstroem, V.; Polivka, T. *J. Phys. Chem. B* **2002**, in press.
(49) Zimmermann, J.; Linden, P. A.; Vaswani, H. M.; Hiller, R. G.; Fleming, G. R. *J. Phys. Chem. B* **2002**, *106*, 9418−9423.
(50) Sharples, F. P.; Wrench, P. M.; Ou, K.; Hiller, R. G. *Biochim. Biophys. Acta* **1996**, *1276*, 117−123.
(51) Martinson, T. A.; Plumley, G. F. *Anal. Biochem.* **1995**, *228*, 123.
(52) Frisch, M. J.; Trucks, G. W.; Schlegel, H. B.; Scuseria, G. E.; Robb, M. A.; Cheeseman, J. R.; Zakrzewski, V. G.; Montgomery, J. A., Jr.; Stratmann, R. E.; Burant, J. C.; Dapprich, S.; Millam, J. M.; Daniels, A. D.; Kudin, K. N.; Strain, M. C.; Farkas, O.; Tomasi, J.; Barone, V.; Cossi, M.; Cammi, R.; Mennucci, B.; Pomelli, C.; Adamo, C.; Clifford, S.; Ochterski, J.; Petersson, G. A.; Ayala, P. Y.; Cui, Q.; Morokuma, K.; Malick, D. K.; Rabuck, A. D.; Raghavachari, K.; Foresman, J. B.; Cioslowski, J.; Ortiz, J. V.; Stefanov, B. B.; Liu, G.; Liashenko, A.; Piskorz, P.; Komaromi, I.; Gomperts, R.; Martin, R. L.; Fox, D. J.; Keith, T.; Al-Laham, M. A.; Peng, C. Y.; Nanayakkara, A.; Gonzalez, C.; Challacombe, M.; Gill, P. M. W.; Johnson, B. G.; Chen, W.; Wong, M. W.; Andres, J. L.; Head-Gordon, M.; Replogle, E. S.; Pople, J. A. *Gaussian 98*, revision A.9; Gaussian, Inc.: Pittsburgh, PA, 1998.
(53) Martin, C. H.; Birge, R. R. *J. Phys. Chem. A* **1998**, *102*, 852−860.
(54) Hudson, B. S.; Birge, R. R. *J. Phys. Chem. A* **1999**, *103*, 2274−2281.
(55) Birge, R. R.; Zgierski, M. Z.; Serrano-Andres, L.; Hudson, B. S. *J. Phys. Chem. A* **1999**, *103*, 2251−2255.
(56) Dolan, P. M.; Miller, D.; Cogdell, R. J.; Birge, R. R.; Frank, H. A. *J. Phys. Chem. B* **2001**, *105*, 12134−12142.
(57) Kusnetzow, A.; Singh, D. L.; Martin, C. H.; Barani, I.; Birge, R. R. *Biophys. J.* **1999**, *76*, 2370−2389.
(58) Stuart, J. A.; Vought, B. W.; Zhang, C. F.; Birge, R. R. *Biospectroscopy* **1995**, *1*, 9−28.
(59) Tallent, J. R.; Birge, J. R.; Zhang, C. F.; Wenderholm, E.; Birge, R. R. *Photochem. Photobiol.* **1992**, *56*, 935−952.
(60) Tallent, J. R.; Hyde, E. Q.; Findsen, L. A.; Fox, G. C.; Birge, R. R. *J. Am. Chem. Soc.* **1992**, *114*, 1581−1592.
(61) Barlow, R.; Birge, R.; Kaplan, E.; Tallent, J. *Nature* **1993**, *366*, 64−66.
(62) Masthay, M. B.; Findsen, L. A.; Pierce, B. M.; Bocian, D. F.; Lindsey, J. S.; Birge, R. R. *J. Chem. Phys.* **1986**, *84*, 3901−3915.
(63) Mortensen, O. S.; Svendsen, E. N. *J. Chem. Phys.* **1981**, *74*, 3185−3189.
(64) Klamt, A.; Shuurmann, G. *Perkin Trans.* **1993**, 799−812.
(65) Miertus, S.; Scrocco, E.; Tomasi, J. *Chem. Phys.* **1981**, *55*, 117−129.
(66) Miertus, S.; Tomasi, J. *Chem. Phys.* **1982**, *65*, 239−245.
(67) Birge, R. R. One-photon and two-photon excitation spectroscopy. In *Ultrasensitive laser spectroscopy*; Kliger, D. S., Ed.; Academic Press: New York, 1983; pp 109−174.
(68) Birge, R. R.; Zhang, C. F. *J. Chem. Phys.* **1990**, *92*, 7178−7195.
(69) Monson, P. R.; McClain, W. M. *J. Chem. Phys.* **1970**, *53*, 29−37.
(70) Bennett, J. A.; Birge, R. R. *J. Chem. Phys.* **1980**, *73*, 4234−4246.
(71) Birge, R. R.; Bennett, J. A.; Pierce, B. M.; Thomas, T. M. *J. Am. Chem. Soc.* **1978**, *100*, 1533−1539.
(72) Pierce, B. M.; Bennett, J. A.; Birge, R. R. *J. Chem. Phys.* **1982**, *77*, 6343.
(73) Dick, B.; Hohlneicher, G. *J. Chem. Phys.* **1982**, *76*, 5755−5760.
(74) Birge, R. R.; Zhang, C. F. *J. Chem. Phys.* **1990**, *92*, 7178−7195.
(75) Ren, L.; Martin, C. H.; Wise, K. J.; Gillespie, N. B.; Luecke, H.; Lanyi, J. K.; Spudich, J. L.; Birge, R. R. *Biochemistry* **2001**, *40*, 13906−13914.
(76) *Cis−trans isomeric carotenoids, vitamin A, and arylpolyenes*; Zechmeister, L., Ed.; Academic Press: New York, 1962.
(77) Honig, B.; Dinur, U.; Birge, R. R.; Ebrey, T. G. *J. Am. Chem. Soc.* **1980**, *102*, 488−494.
(78) McRae, E. G. *J. Phys. Chem.* **1957**, *61*, 562−572.